Atmos. Meas. Tech., 19, 3231–3251, 2026
https://doi.org/10.5194/amt-19-3231-2026

Atmospheric Measurement Techniques
Open Access
EGU

Development and application of the Ascent-Drift-Descent Radiosonde System (ADDRS)

Xiaozhong Cao[1], Qiyun Guo[2,3,4], Haowen Luo[2,3,4], Jincheng Wang[5], Rongkang Yang[2,3,4], Die Xiao[6], Yinfeng Liu[7], Zhongliang Sun[8], Shijun Liu[9], Sijie Chen[10], Anfan Huang[2,3,4], Guo Jianping[11], and Peng Zhang[2,3,4]

[1]China Meteorological Administration, Beijing, China
[2]Meteorological Observation Centre of China Meteorological Administration, Beijing, China
[3]State Key Laboratory of Environment Characteristics and Effects for Near-space, Beijing, China
[4]Engineering Technology Research Center for Meteorological Observation of CMA, Beijing, China
[5]CMA Earth System Modeling and Prediction Centre (CEMC), Beijing, China
[6]Hunan Key Laboratory of Near-space Meteo-ballon Materials and Technology,
Zhuzhou Research & Design Institute Co, Ltd, Zhuzhou, China
[7]Beijing Huayun Orient Detection Technology Co, Ltd., Beijing, China
[8]Allystar Technology (Shenzhen) Co. LTD., Shenzhen, China
[9]Department of Advanced Technology Training of China Meteorological Administration, Beijing, China
[10]National Satellite Meteorological Centre of China Meteorological Administration, Beijing, China
[11]Chinese Academy of Meteorological Sciences, Beijing, China

Correspondence: Xiaozhong Cao (caoxzh@cma.gov.cn) and Peng Zhang (zhangp@cma.gov.cn)

Received: 29 April 2025 – Discussion started: 17 June 2025
Revised: 4 March 2026 – Accepted: 1 April 2026 – Published: 21 May 2026

Abstract. Balloon-borne radiosonde observations constitute a crucial component of meteorological sounding, which conducts a ground to upper-air "ascent phase" sounding. This paper introduces the Ascent-Drift-Descent Radiosonde System (ADDRS), an innovative system characterized by three observation phases – "Ascent-Drift-Descent" (ADD) – in which all three phases of sounding observation are executed through single balloon launch. Several key technologies were successfully developed, including the carrier (dual-mode balloon), the payload (System-on-Chip (SoC) module for radiosonde), Ground to upper-air data reception and control command transmission and data processing framework based on "Internet cloud + Instrument terminal" was established. Data quality control methods and data assimilation techniques of ADDRS were also developed. An interactive experiment encompassing observations and forecasting was conducted to evaluate the quality of experimental data at each phase of ADDRS. Numerical assimilation and forecasting experiments showed a positive (albeit not yet statistically significant) impact on forecast quality for both general cases and for Tropical cyclone cases. The pre-operational launching and assimilation of more than 100 such radiosondes started on 1 July 2024 and provided data over 1 year, and the number of stations continues to grow.

1 Introduction

The upper-air meteorological sounding system (hereinafter referred to as "sounding") constitutes a key element within comprehensive meteorological measurement framework (Ingleby et al., 2016a). It is responsible for gathering data on various meteorological elements such as temperature, humidity, pressure, wind speed, and wind direction from the surface up to heights of 30 km and beyond upper atmosphere (DuBois et al., 2002). This system provides vertically observed meteorological data for weather forecasting, numerical weather prediction, climate projection, scientific research, and the inspection and calibration of ground-based remote sensing equipment (Seidel et al., 2009; Fujiwara et al., 2025). The integration of radiosonde technology with balloon-borne soundings emerged in the 1930s, with early

operational systems deployed in the 1940s; this technology has since served as a primary tool for direct measurements of upper-air meteorological elements below 30 km and is widely utilized on a global scale (Pettifer, 2009; Gallice et al., 2011).

For nearly a century, these radiosondes have utilized the direct measurement method of "one balloon launched, one profile". The radiosonde ascends at a certain speed with the balloon expanding in volume due to decreasing air pressure as altitude increases. Upon reaching a specific altitude, the balloon bursts, concluding the measurement process. This methodology confines effective observations to the radiosonde's ascent phase (Haig and Lally, 1958). The disposable nature of radiosondes and balloons necessitates significant costs for multiple deployments. Consequently, economic constraints have led to reductions in sounding operations, such as Russia's temporary reduction of launches from twice to once daily in 2015, impacting the forecasting accuracy of numerical prediction models across Northern Hemisphere countries (Ingleby et al., 2016b).

In recent decades, satellite soundings have played an increasing role in Numerical Weather Prediction (NWP) and are now the observations contributing most to forecast skill (Bauer et al., 2015; Bormann et al., 2019; WMO, 2024a). While radio occultation data has gained importance as a reference standard (Bauer et al., 2014), radiosonde profiles still provide an important contribution to forecast skill, help with the calibration and validation of satellite soundings and allow independent verification of forecast fields. But the temporal resolution of global radiosonde observations data remains limited, posing a significant challenge to its capacity in fulfilling the requirements of routine forecasting. A notable concern arises from the scarcity of direct measurement data during periods characterized by frequent severe convective activity, particularly in the hours immediately following noon. Several studies have demonstrated that the frequent acquisition of descent radiosonde data can enhance the accuracy of numerical weather forecasting. Some multi-year studies (Cohn et al., 2013; Wang et al., 2015) suggest that assimilation of dropsonde data can reduce hurricane trajectory short-range forecast errors by 10 %–15 %. However other studies reviewed by Majumdar (2016) show less impact.

Additionally, several institutions are actively investigating techniques to obtain multiple radiosonde data points from a solitary balloon launch. Illustrative projects include the multidisciplinary analysis of the African monsoon and the measurement system research and forecasting experiments conducted in the Asia-Pacific region, which utilize balloons to conduct drop soundings as they drift with stable upper-air winds over the ocean (Raman et al., 2011; Johnson et al., 2024). Similarly, the Centre National d'Etudes Spatiales (CNES) of the French Space Agency, has developed a Super Pressure Balloon (SPB) capable of floating in the stratosphere for over three months (Hertzog et al., 2021). Additionally, the Tata Institute of Fundamental Research Balloon Facility (TIFR-BF) in India has also contributed to this field by developing comparable systems (Anand et al., 2021; Vernier et al., 2018, 2022). Early stratospheric balloon systems encountered doubts concerning their long-term feasibility for operational data collection, attributable to cost and ascent rate limitations (WMO, 2025). Additionally, slower ascent rates result in radiative errors issue. However, for wind vectors, especially crucial upper-level winds, GPS-based positioning provides high-precision data less affected by the ascent rate. The development of a new generation of commercial balloon systems has been changing this landscape. Studies by Venkat Ratnam et al. (2014) and Ingleby et al. (2022) looked at the quality and value of radiosonde descent data. This paper introduces a new sounding technology – the Ascent-Drift-Descent Radiosonde System (ADDRS). This system can improve the spatial and temporal frequency of soundings and provides an additional vertical profile as well as maintaining cost-effective, which acquires radiosonde measurement data throughout three phases – "Ascent-Drift-Descent" (ADD) – all with a single balloon launch (Cao et al., 2019, 2022).

2 Synopsis of the Ascent-Drift-Descent Radiosonde System (ADDRS)

The ADDRS was developed by the Meteorological Observation Centre of the China Meteorological Administration (MOC of CMA) with other relevant organizations in China (hereinafter referred to as the "ADDRS research team"). It undertakes a three-phase upper-air measurement (Fig. 1).

The ADDRS primarily consists of the "ADD" subsystem and the ground operation control subsystem, as shown in Table 1 and Fig. 2. The "ADD" subsystem encompasses a dual-mode balloon with a parachute, a drifting controller, and a radiosonde. The dual-mode balloon features a design where one balloon embedded within another, both made from a latex material similar to that of meteorological sounding balloons and filled with hydrogen. Upon inflation and launch of the dual-mode balloon, the "ADD" subsystem at a rate of ascent between 5 and 7 $\mathrm{m\,s^{-1}}$ (WMO, 2025). As it rises, the external air pressure decreases, causing the balloon to expand. At the predetermined altitude (generally between 28 and 30 km), the outer balloon bursts due to its expanding volume, marking the conclusion of the ascent phase measurement. Given that the outer balloon bursts within the stratosphere, where vertical air movement is minimal, horizontal movement becomes predominant. The inner balloon does not burst, and the buoyancy of the inner balloon attains equilibrium with vertical stability, starting the drift phase.

After drifting for a predefined duration, which may vary from a couple of hours to over 10 h, the drifting controller separates the inner balloon from the rest of the ADDRS equipment, thereby terminating the drift phase. The parachute is promptly deployed, facilitating the radiosonde

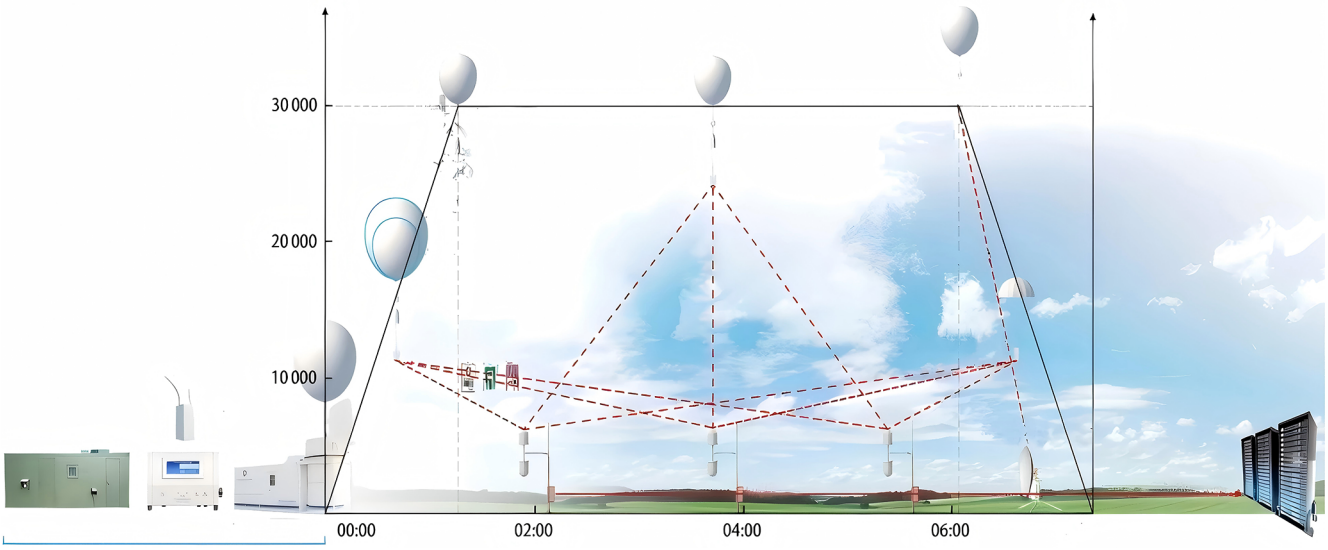

Figure 1. Pre-operational principle diagram of the Ascent-Drift-Descent Radiosonde System (ADDRS).

Table 1. Main instruments and key functions of ADDRS.

No.	Subsystem	Instruments	Key Function
1	"ADD" subsystem	dual-mode balloon	"outer balloon" as ascent carrier, "inner balloon" as drift carrier
2		parachute	parachute as the carrier of the descent phase
3		drifting controller	Adaptive control of drift and descent
4		radiosonde	The temperature, pressure, humidity, wind measurement meet the demand for long-term stratospheric observation
5	Ground operation control subsystem	Launch station	Manned radiosonde inspection, ground check, balloon inflation, and other balloon tasks
6		Multichannel sounding receiver	8 channels receive radiosonde data simultaneously
7		control command transmitter	In a weather-sensitive area without a station, the inner balloon can be detached and the descent started
8		operation management system	Real-time acquisition, transmission, quality control, and timely delivery of control instructions for ADDRS data, providing real-time high-quality data to weather analysis and numerical prediction models

in collecting data during the descent phase, while acting as its carrier. This descent persists until the equipment touches down, thereby completing the final phase of the "ADD" process. At this point, ADDRS has successfully completed the three-phase "Ascent-Drift-Descent" measurement.

The ground operation control subsystem of ADDRS comprises four main components in Table 1. The launch station operates with a high degree of automation for scheduled sequences, though the critical procedure for inflating the inner balloon to achieve drift requires operator supervision. Full automation of this process is under active development.automated. Ground data-receiver can also be placed at the balloon launch station. However, its layout and function differ from the operational-ground data-receiver. Due to the ADDRS drift phase, the horizontal distance between the descent point of the radiosonde and its launch point can exceed 500 km, while radiosonde data reception has a maximum linear transmission distance of around 200–300 km. Therefore, the traditional single-station, point-to-point radio communication mode of radiosondes is inadequate for AD-

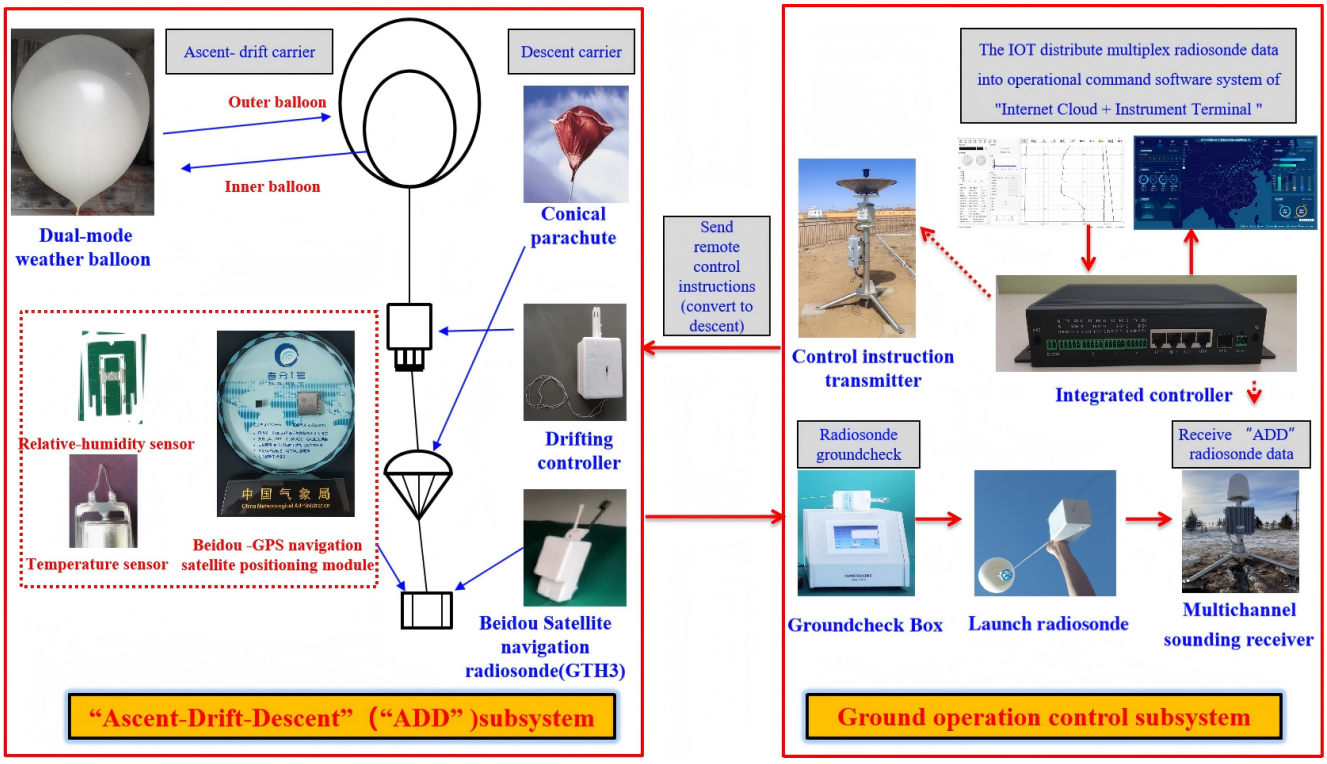

Figure 2. Schematic representation of the equipment composition for ADDRS.

DRS data reception. Thus, the ground to upper-air communication system has been upgraded from point-to-point to a multiple-to-multiple model. In areas through which the radiosonde's ADD phases may pass, ground data-receivers are strategically deployed. This configuration enables multiple ground data-receivers to concurrently receive data from a single radiosonde or alternatively, a single receiver to capture data signals from several radiosondes simultaneously. Consequently, the ground data-receiver is designed as a P-band 8-channel parallel data receiver, capable of receiving data from multiple radiosondes simultaneously. Additionally, control command transmitters are located at the ground station and other locations. These transmitters send control instructions from the ground to the drifting controller in the air through uplink communication. This system allows for the adjustment of the drift phase elevation, termination of the drift phase, and switching to the descent phase measurement as needed.

The operation management system acts as the brain of the entire ADDRS system. Multiple ground data-receivers and control command transmitters are connected to the operation management system by the Internet. These ground data-receivers continuously transmit data to the operation management system in real-time for processing, display, and storage. Based on the ADDRS trajectory and specific weather and climate conditions, comprehensive decision-making allows the operation management system to transmit control instructions to control command transmitters which then relay them to the drifting controller in the air to execute the desired functions.

The "Internet cloud + Instruments terminal" architecture enables real-time, efficient, and bidirectional communication across the entire network during the "ADD" phases. This configuration supports the seamless real-time acquisition, transmission, and quality control of ADDRS data while ensuring rapid data delivery for weather forecasting. Consequently, it enhances the timeliness and availability of radiosonde data for forecasting purposes.

3 Critical scientific problems

3.1 Carrier technology

3.1.1 Study on the influence of atmospheric environment on the net lift power of balloons

A multitude of meteorological factors, encompassing air temperature, air pressure, solar radiation, and other external environmental conditions, coupled with the gas volume of the outer balloon directly influences its net lift and burst altitude. Variations in pressure and temperature within the outer balloon, induced by external meteorological conditions, interact with the expansion dynamics of the inner balloon. These factors, in conjunction with the optimum volume of

the inner balloon, collectively influence the altitude during the drift phase and the static equilibrium of the inner balloon. Consequently, controlling the hydrogen inflation volume in the dual-mode balloon presents a significant challenge.

The ADDRS research team conducted an in-depth theoretical analysis of the ascent and drift processes of the dual-mode balloon, focusing on three areas: upper atmosphere model expansion, the balloon's dynamic equation, and a thermodynamic model. This study led to the development of a coupling model that accounts for the effects of atmospheric conditions on the balloon's net lift (from now on referred to as the "coupling model") (Liu et al., 2022b). This model provides a theoretical foundation for determining the net lift force, ascent velocity, and target burst altitude of the dual-mode balloon, enabling precise control of the mass of air in the balloons in the dual-mode balloon under varying meteorological conditions.

Table 2 presents data from six stations (Changsha, Wuhan, Anqing, Yichang, Nanchang, and Ganzhou) situated along the middle and lower reaches of the Yangtze River in 2021. And based on the sounding balloon observation data in Guangdong from August 2022 to October 2023, the optimum volume capacities of related factors of the inner and outer balloons of the dual-mode sounding balloon on the success rate of the drift were studied, and a reasonable inflation scheme was established to improve the success rate of the drift. The research shows that the theoretical inflation amount of the inner balloon for drifting at the expected height is 55.6 mol. Affected by day and night conditions, the inflation amount during the day should be controlled at 52.6 ± 2 mol, and at night, it should be controlled at 57.6 ± 2 mol. The burst height of the outer balloon has a significant impact on the success rate of the drift. When the burst height of the outer balloon is within the expected height, the success rate of the drift can reach 82 %. The success rate of the drift during the day is higher than that at night, and the success rate under clear sky conditions is higher than that under cloudy and rainy conditions. Under rainy conditions, the success rate of the drift is only 50.2 %. After verification, the success rate of the drift can reach 93.5 % by adopting the reasonable inflation scheme (Xu et al., 2025).

3.1.2 Performance improvement of the double-layer balloon

The ascent phase of meteorological sounding typically lasts between 1.5 and 2 h. However, during the ADD process, the inner balloon of the dual-mode balloon is exposed to low temperatures, intense ultraviolet radiation, and high ozone concentrations for several hours or even up to 10 h. To address these challenges, the ADDRS research team conducted formulation tests to enhance the inner balloon resistance to these environmental factors, with a particular emphasis on natural latex modification, cold resistance, and anti-aging systems. Considering that latex hot air aging performance improves air tightness and balloons are exposed to prolonged sun exposure and hydrogen loss, the incorporation of a specific latex compound was found to augment durability. Figure 3a and b show that the addition of latex formulas had minimal impact on the latex viscosity and the balloon appearance while improving its tensile strength and thermal aging resistance. Figure 3c and d demonstrate that butyl oleate exhibits the lowest reduction in low-temperature burst performance after water extraction and accelerated aging, making it the best-performing cold-resistant agent. Consequently, this agent was integrated into the formula to bolster cold resistance. For the anti-aging system, illustrated in Fig. 3e and f, nano zinc oxide, which can be diluted directly with water to replace traditional zinc oxide, was used. Additionally, we incorporated antioxidants to enhance the balloons' resistance against ultraviolet and ozone degradation. These formula improvements extend the inner balloon lifespan under harsh conditions of low temperature, intense UV radiation, and high ozone levels. This enhanced durability has been applied to the inner balloon, resulting in an extended service life and a high success rate during the drift phase (Zhu et al., 2021; Shen et al., 2020).

3.2 Payload technology

3.2.1 Performance improvement of the radiosonde

Due to ADDRS operates effectively across all three phases of the ADD process, requiring a minimum operation time of 6 h. This extended operation necessitates a larger-capacity battery for the ADDRS radiosonde. Additionally, the radiosonde's weight affects the balloon's inflation volume, making it essential to reduce the radiosonde's weight where possible. Therefore, an integrated, lightweight, and low-power radiosonde is crucial, and the ADDRS research team developed a specialized SoC (System on Chip) module (named Equinox I) for CMA's GTH type of Beidou-based radiosonde.

The GTH3 employs a specialized SoC module of meteorological sounding and utilizes a multi-layer board design and miniaturized components to reduce the size, weight, and power consumption. Compared to the previous operational radiosonde (GTS12 radiosonde, WMO BUFR code: 201), the GTH3 radiosonde (WMO BUFR code: 206) significantly reduce the overall size, weight, and power consumption of the device. Furthermore, the amount of plastic and toxic materials in the circuit boards has also been substantially reduced (Table 3).

The GTS12 and GTH3 radiosonde use the same PTU sensor, P (MEMS piezo-resistive), T (adopting self-developed NTC bead thermistor (reduced from diameter ≤ 1 to ≤ 0.4 mm) volume reduction, higher sensitivity), U (capacitive thin-film polymer humidity sensor). The difference lies in that "Instrumentation and Methods":

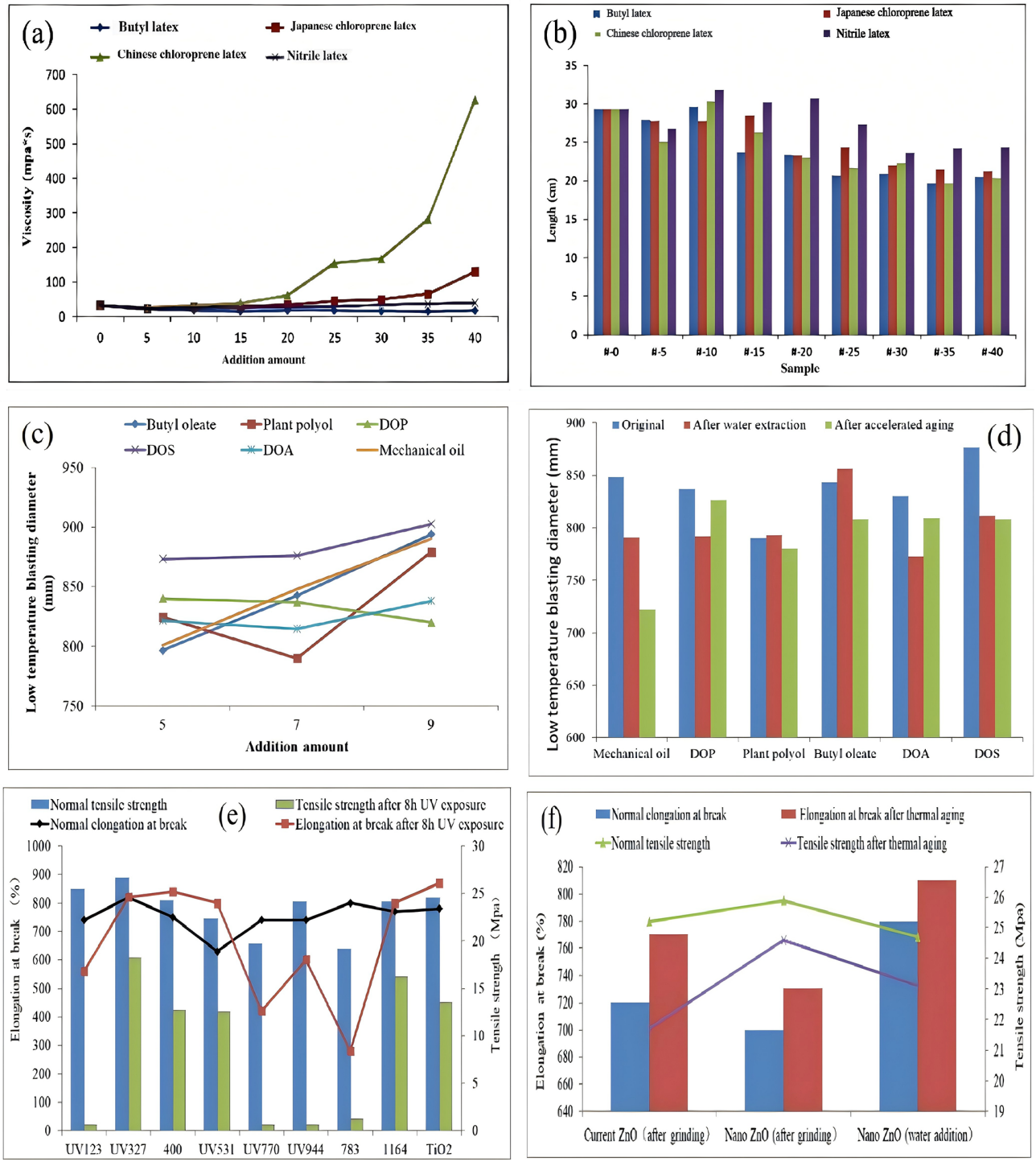

Figure 3. Modification test of natural latex in the inner sphere: **(a)** four types of modified natural latex materials – Butyl latex, Japanese chloroprene latex, Chinese chloroprene latex, and Nitrile latex – were screened and added to natural latex using the homogenization method. **(b)** Physical properties of the modified natural latex pellet samples were evaluated for operation and thermal aging tensile testing. **(c)** Butyl oleate, Plant polyol,DiOctyl Phthalate (DOP), DiOctyl Sebacate (DOS), DiOctyl Adipate (DOA), and mechanical oil were added to natural latex as cold resistance agents. Cold resistance system test: the blasting diameters of six types of cold-resistant samples were tested using low-temperature blasting instruments at −85 °C. **(d)** Low-temperature blasting diameters were measured for six types of raw, water-pumped, and aged samples with seven parts of cold-resistant agents added. Anti-aging system test: **(e)** comparison of tensile properties among nine anti-aging agents – UV327, UV400, UV531, UV1164, and TiO2 filler – with 0.2 parts of one-component anti-aging agent after 8 h of operation and ultraviolet aging. **(f)** Comparison of tensile properties after ozone aging between Nano ZnO and ZnO.

Table 2. Inflate test results based on coupling model.

Inflatable mode	Effective launch times	Drift number of times	Drift success rate	≥ 4 h number of times	≥ 4 h success rate
Algorithm software	611	479	78.40 %	436	71.36 %

Table 3. Comparison of parameters among RS41, GTH3 and GTS12 radiosonde.

Radiosonde type	Positioning method	Volume (mm^3)	Weight (g)	Transmitting power (mW)	Working time (min)	Data Transmission Rate (bps)	Battery Weight (g)	Foam Packaging Weight (g)	Circuit boards Weight (g)
GTS12 radiosonde	Radar positioning	$190 \times 90 \times 245$	< 400	≤ 400	> 120	1200	< 250	< 70	< 80
GTH3	Equinox I	$155 \times 65 \times 60$	< 120 (for one profile)	≤ 100	> 240	Optional, 2400, 4800, 9600	< 40	< 30	< 50
		$155 \times 65 \times 60$	< 170 (for "ADD" three phase profile)	≤ 100	> 640		< 90	< 30	< 50
Vaisala RS41	*u*-blox G7020	$155 \times 60 \times 46$	109	60	> 240	4800	76	–	–

- For P [Design the temperature compensation circuit and establish the correction equation by fitting the sensor characteristic surface through multiple temperature segments and multiple pressure points to achieve higher measurement accuracy.]
- For T [Optimize the installation structure, included Angle and lead length through simulation analysis, and effectively reduce the influence of solar radiation by improving the installation structure and coating process.]
- For U [Optimize the Temperature compensation Correction Algorithm and humidity hysteresis Correction Algorithm for Humidity sensors]

The GTH3 participated in WMO UAII2022 (Upper-Air Instrument Intercomparison Campaign organized by the World Meteorological Organization (WMO) and co-organized by the Deutscher Wetterdienst (DWD) in 2022) with the results shown in Table 4. It is suitable for applications in ORUC (Operational and Research Use in Climatology), including aeronautic meteorology, near/ultra-short-term forecasting, global numerical weather prediction, and real-time monitoring (WMO, 2024b).

3.2.2 Drifting controller

The drifting controller can be considered part of the ADDRS payload. It connects to an inner balloon above and a parachute and radiosonde below. The controller fuses a wire with an instant high electric current, triggering the mechanical device to disconnect the parachute and the radiosonde. The controller serves two main functions during the drift phase:

1. Similar to the Windborne system, it is equipped with a ballast-dropping mechanism to control its weight, allowing the inner balloon to better adapt to changes in altitude.
2. Separate the inner balloon from the other sounding equipment (parachute and radiosonde). Moreover, the drifting controller can also initiate the fuse based on predetermined control rules, such as altitude limits (≤ 18 km), specified time, the latitude and longitude of a designated area, or upon receiving commands from the ground. This action can be taken before the drifting balloon is about to enter the specified area or approach the maximum drift height. As a result, it will effectively end the drift phase, separating the parachute and radiosonde from the balloon.

3.3 Receiving radiosonde data and sending control instructions technology

The ADDRS ground data-receiver utilizes a high-gain, low-power, ultra-compact omnidirectional antenna, along with super-heterodyne architecture and multiple communication protocol algorithms, including time division multiple access, frequency division multiple access, and code division multiple access (Gong et al., 2021). It supports various frequency modulation modes and achieves a receiving sensitivity of better than -120 dBm (at 2400 bps), effectively addressing self-interference issues in multi-channel radiosonde data reception. Additionally, the system incorporates narrowband wireless communication technology to improve low-elevation reception when the radiosonde drops below the receiving antenna's height, facilitating broad-area coverage

Table 4. The evaluation results of GTH3 radiosonde temperature, pressure, relative humidity, wind and geopotential height in WMO Instruments and Observation Methods Report No. 143 (p. 150, WMO, 2024b). (Note: The data are in the form of $(\Lambda_{c,L})^{\delta_{c,L}}_{\sigma(\delta)} \pm \epsilon_{c,L}$, where $\Lambda_{c,L}$ represents the individual measurement root mean square error, $\epsilon_{c,L}$ denotes the measurement uncertainty, $\delta_{c,L}$ is the measurement error, and $\sigma(\delta)$ indicates the measurement standard deviation. The planetary boundary layer (PBL) ranges from surface to 2 km; the free troposphere (FT) ranges from 2 km to the tropopause 12 km; the upper troposphere/lower stratosphere (UTLS) ranges from 7 to 17 km; the middle and upper stratosphere (MUS) is above 17 km up to the bursting point of the sounding balloon.)

Time	Height	Atmospheric temperature [K]	Relative humidity [%RH]	Geopotential height [m]	Pressure [hPa]	Wind (horizontal) direction [°]	Wind (horizontal) speed [m s^{-1}]	Wind (horizontal) vector [m s^{-1}]
Day	PBL	$0.18^{-0.05}_{0.17} \pm 0.03$	$7.00^{-5.43}_{4.41} \pm 0.74$	X	X	X	X	X
	FT	$0.12^{+0.05}_{0.11} \pm 0.04$	$8.75^{-3.50}_{8.02} \pm 0.60$	$5.9^{+2.0}_{5.5} \pm 1.8$	$0.4^{-0.0}_{0.4} \pm 0.1$	$3.6^{-0.4}_{3.6} \pm 0.2$	$0.2^{-0.0}_{0.2} \pm 0.0$	$0.3^{+0.2}_{0.1} \pm 0.0$
	UTLS	$0.09^{+0.01}_{0.08} \pm 0.03$	$7.73^{-1.55}_{7.58} \pm 0.40$	$13.2^{+10.0}_{8.6} \pm 3.8$	$0.4^{-0.3}_{0.2} \pm 0.1$	$2.5^{-0.2}_{2.5} \pm 0.3$	$0.2^{-0.0}_{0.2} \pm 0.0$	$0.3^{+0.2}_{0.2} \pm 0.0$
	MUS	$0.27^{-0.22}_{0.16} \pm 0.10$	$1.69^{+1.48}_{0.82} \pm 0.46$	$29.5^{+23.4}_{17.9} \pm 4.2$	$0.3^{-0.2}_{0.1} \pm 0.0$	$6.1^{-0.4}_{6.1} \pm 0.2$	$1.3^{-0.0}_{1.3} \pm 0.0$	$1.5^{+0.3}_{1.5} \pm 0.0$
Night	PBL	$0.38^{-0.18}_{0.34} \pm 0.05$	$4.72^{+0.74}_{4.66} \pm 0.15$	X	X	X	X	X
	FT	$0.15^{+0.02}_{0.15} \pm 0.02$	$6.41^{+2.16}_{6.03} \pm 0.11$	$5.8^{+0.4}_{5.8} \pm 0.4$	$0.5^{+0.1}_{0.5} \pm 0.2$	$2.6^{-0.2}_{2.6} \pm 0.2$	$0.2^{-0.0}_{0.2} \pm 0.0$	$0.2^{+0.2}_{0.1} \pm 0.0$
	UTLS	$0.12^{+0.06}_{0.10} \pm 0.05$	$6.82^{+3.70}_{5.74} \pm 0.26$	$11.5^{+7.7}_{8.6} \pm 3.4$	$0.3^{-0.1}_{0.2} \pm 0.1$	$2.4^{-0.1}_{2.4} \pm 0.1$	$0.2^{+0.0}_{0.2} \pm 0.0$	$0.2^{+0.2}_{0.1} \pm 0.0$
	MUS	$0.10^{-0.03}_{0.10} \pm 0.02$	$1.71^{+1.54}_{0.74} \pm 0.28$	$26.7^{+20.7}_{16.8} \pm 4.2$	$0.1^{-0.1}_{0.1} \pm 0.0$	$4.5^{-0.6}_{4.4} \pm 0.2$	$0.2^{-0.0}_{0.2} \pm 0.0$	$0.4^{+0.3}_{0.3} \pm 0.0$

with a visual range radius for upper-air coverage of at least 200 km. The receiver can adapt to diverse application scenarios, such as fixed stations, vehicles, and ships. With an average data reception rate of 99.7 %, the ground receiver at the Anqing station has demonstrated an impressive maximum reception distance of up to 487 km.

Unlike the one-way (downlink) communication mode used in radiosonde systems, the ADDRS control command transmitter can send ground instructions to the drifting controller, with a linear communication range extending beyond 300 km. This capability allows for precise control over the drifting controller to execute actions such as releasing counterweights or separating the balloon from the parachute and radiosonde, enabling the radiosonde to conduct drift phase measurements within the target area (Liu et al., 2021). During field tests, over ten balloon discharge control commands were successfully transmitted, with the farthest reaching 403 km.

3.4 "ADD" measurement technology

The details of the ADD measurement method are outlined by Cao et al. (2019). The ascent phase measurement technique adheres to the guidelines outlined in the CMA technical specification. The primary research focus of the ADDRS is on the measurement techniques for the drift and descent phases.

3.4.1 Temperature measurement method in the drift phase

During the drift phase of ADDRS, the inner sphere of the dual-mode balloon moves with the horizontal airflow in the stratosphere. The radiosonde's vertical movement, with the surrounding atmosphere, is minimal and it can be approximately considered as drifting with the horizontal wind. The effect of radiation on the temperature sensor during this phase is greater than during the ascent and descent phases, leading to considerable measurement errors that are challenging to correct using general quality control algorithms.

Given the unique conditions of stratospheric air temperature measurement, the ADDRS research team employs a multi-physical field, fluid-structure coupled computational fluid dynamics (CFD) approach to model the behavior of the temperature sensor in high-altitude, low-wind-speed environments. This model calculates the flow and the temperature field, accounting for radiation effects based on sun elevation, ventilation, sensor size, and surface reflectivity. To ensure broad applicability, neural networks, and other mathematical methods are used to fit the extensive simulation data, yielding practical error-correction equations (Yang et al., 2014).

Considering that there may be discrepancies between CFD simulations and real environmental conditions, the ADDRS research team uses instruments such as low-pressure wind tunnels and solar simulators to create an experimental platform. This setup simulates ventilation, air density, and solar radiation conditions during the drift phase, allowing for the measurement of temperature errors due to solar radiation. These measurements verify and refine the simulation-based error correction equations (Yang et al., 2022).

3.4.2 Vertical wind data during the parachute descent

Currently, due to the pendulum effect, vertical wind measurements cannot be performed in balloon-borne soundings. The parachute-drop wind measurement model established by the

WMO and NCAR does not address vertical wind measurement directly (Wang et al., 2015), instead assuming a zero vertical wind speed. This model assumes that the parachute-drop system is influenced only by gravity and vertical resistance, omitting other factors like buoyancy, additional forces, and parachute rotation during descent. This limitation prevents the analysis of vertical wind and also affects the accuracy of horizontal wind field calculations (Ingleby et al., 2022).

Therefore, the ADDRS research team developed a more comprehensive vertical wind measurement model by considering all relevant forces acting on the balloon-launched and parachute descent dropsonde system, utilizing the domestic Beidou-based radiosonde, shows significant promise. The Beidou-based radiosonde demonstrated acceptable accuracy during both ascent and descent phases compared to the RS92 standard. The key advantages identified were the ability to perform temporally intensive sounding observations (effectively obtaining an "ascent" and "descent" profile from one launch) and the potential to spatially expand coverage through the drift of the parachute, allowing for a "one-station launch, multi-station reception" model. This technology aligns with the trend towards automated, quantitative remote sensing in meteorological observation (Guo et al., 2018). The string length between the balloon/parachute and the GTH3 radiosonde is standardized at 30 meters in manual launches. This length helps reduce sensor exposure to balloon wake effects but amplifies pendulum motion in wind data. More than ten comparative tests were carried out for the selection of the conical parachutes. The oscillation angle of conical parachute is less than 1°, which can ensure the rationality of the Gaussian filtering correction filter window for the horizontal wind in the descent phase. Meanwhile, a larger main parachute size can reduce the descent speed. Therefore, without considering the cost, a "large conical parachute" is recommended for the descent phase detection of ADDRS. And make sure the parachute area should be tailored to match the radiosonde weight. The descent phase of ADDRS could achieve a low-level descent speed of $6 \pm 1\,\mathrm{m\,s^{-1}}$ can be achieved in UTLS (upper troposphere and lower stratosphere (7–17 km), and a swing angle below 5°, as well as a vertical wind measurement uncertainty of less than $1\,\mathrm{m\,s^{-1}}$. These findings demonstrate that the model is effective for calculating vertical wind.

4 Field experiments and data quality verification

4.1 Field experiment in the middle and lower reaches of the Yangtze River Region

From 2019 to 2021, ADDRS conducted field tests and application research across a wide area in the middle and lower reaches of the Yangtze River in China. The research focused on measurement data processing methods, quality control algorithms, and application technologies across diverse scenarios. The ADDRS radiosondes were launched from six stations. They were Anqing, Wuhan, Yichang, Nanchang, Changsha, and Ganzhou, which located in Anhui, Hubei, Jiangxi, and Hunan provinces. A total of 14 ground radiosonde data receivers were strategically positioned around these six stations, spaced approximately 150 km apart. The test covered an area of $600\,000\,\mathrm{km^2}$, as shown in Fig. 4, and show a trajectory for ADDRS at the Anqing station at 12:00 UTC on 11 July 2021.

During the 13-month experimental period, 3177 ADDRS launches were conducted, with 3012 classified as effective launches, of which 2369 achieved successful drifting. Among these, 2136 launches resulted in drifting for more than 4 h. The overall drifting success rate was 79 %, with a 4 h drifting success rate of 71 % (Fig. 5).

From March to September 2021, 2427 "ADD" radiosonde launches were conducted, with 2,281 classified as effective launches, of which 1772 achieved successful drifting. Among these, 1587 launches resulted in drifting for more than 4 h. The overall drifting success rate was 78 %, with a 4 h drifting success rate of 70 %. The 1772 successful drifts were analyzed (Fig. 6), and 937 were successful during the daytime, accounting for 53 %. The successful nighttime drifting was 835 times, accounting for 47 %, somewhat worse than the daytime performance. The drift heights ranging from < 75 hPa (< 18 km) to 15–10 hPa (28–32 km) were statistically analyzed. The proportion of outer balloon explosion heights within 15–10 hPa (28–32 km) was the largest (43 %). And the proportion of 20–15 hPa (26–28 km) is 40 %, the proportion of 30–20 hPa (24–26 km) is 9 %, and the total proportion of beyond 30 hPa is 92 %. Therefore, The drift height meets the GBON requirement of attaining at least 30 hPa for a majority of ascents, with a subset of ascents also reaching the 10 hPa level (WMO, 2020).

Due to the limited availability of high frequency, continuous measurement data for the stratospheric atmosphere, experiments were conducted in the middle and lower reaches of the Yangtze River to obtain direct measurement data with high spatial and temporal density (Zhang et al., 2021b). The simulated and observed trajectories are represented by red and black, respectively (Fig. 7). A color gradient based on pressure altitude is used to indicate the variation of trajectory height along the path.

The balloons drifting of ADDRS radiosondes data in the above tropopause have been very useful for verification of FY-3D satellite temperature and humidity profiles (Zhou et al., 2023, 2024). And application in observing certain features of gravity waves in the lower stratosphere (He et al., 2024; Yang et al., 2021) and feature extraction and analysis of atmospheric turbulence (Yang et al., 2023).

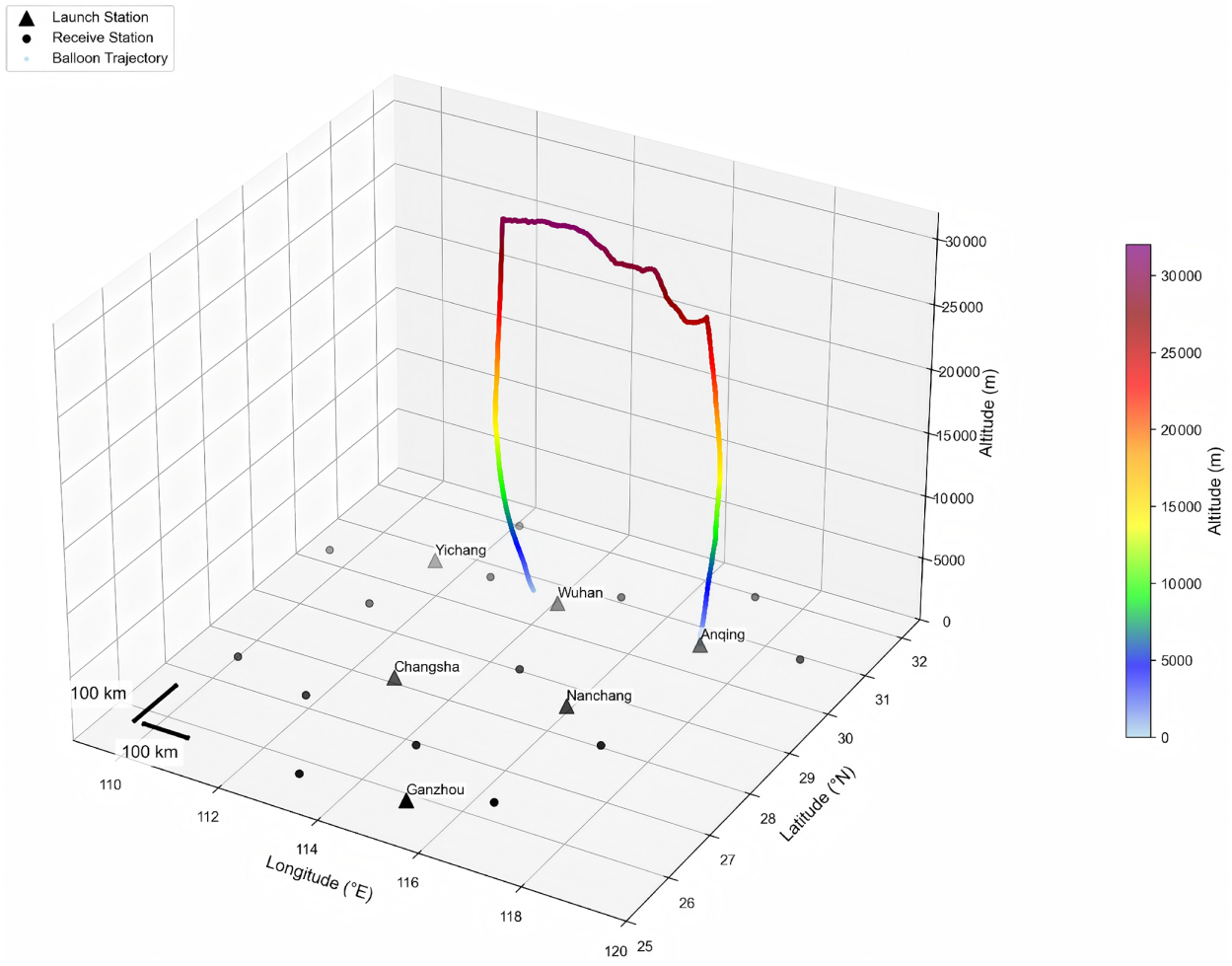

Figure 4. The network distribution of ADDRS and an example of measurement: the trajectory for ADDRS at the Anqing station at 12:00 UTC on 11 July 2021. The black triangles represent balloon launch stations of ADDRS, while the black dots represent ADDRS receiving stations.

4.2 Data quality evaluation

Aiming at the characteristics of high-resolution ADDRS data for quantitative application, the ADDRS research team carefully evaluated ADDRS data using 31 data quality control methods based on the guidelines for CMA technical specification of operation upper-air meteorological observation (Wang et al., 2020). For the data quality of the ascent phase of the ADD radiosonde, refer to the results in Table 4. Additionally, the fifth generation of ECMWF (ERA5) global reanalysis (Hersbach et al., 2020) was used to evaluate the quality of four upper-air radiosonde observations stations' ADDRS data in Guangdong (Zhang et al., 2025a), and Table 5 demonstrates good consistency between the ascent and descent phases for temperature, u-wind, and v-wind (Yao et al., 2026). The conclusion is basically consistent with the results of Table 4.

But for relative humidity (RH), different radiosonde manufacturers may adopt distinct saturation vapour pressure (SVP) equations in calibrating humidity sensors. This difference in the choice of SVP equation can lead to discrepancies in relative humidity measurements among different radiosonde types, especially under low-temperature conditions. The ADDRS radiosonde humidity sensor is calibrated using the (Goff, 1957) SVP equation recommended in earlier WMO publications (WMO, 2012). Moreover, relative humidity from the ERA5 dataset is calculated using the Buck SVP equation. To ensure a more consistent comparison, relative humidity was recalculated from temperature and specific humidity in the ERA5 dataset using the Goff (1957) SVP equation, with the SVP assumed over liquid water only. The results show that the O–A bias and RMSE of relative humidity under low-temperature conditions are reduced and become much more physically reasonable.

The wind data from the drift phase were validated through dedicated experiments involving accelerometers, applying filtering principles consistent with Marlton et al. (2015). However, we note that the discrepancies in the stratospheric drift phase (both wind and temperature) are larger. This is

Table 5. Comparative analysis of after-quality control of ADDRS radiosonde data and ERA5 (O-A).

			U ($m\,s^{-1}$)		V ($m\,s^{-1}$)		T (K)		RH (% RH)	
			bias	SD	bias	SD	bias	SD	bias	SD
Ascent	Day	Above tropopause	0.03	1.73	0.11	1.91	−0.4	1.04	–	–
		Below tropopause	0.13	1.41	0.08	1.47	0.04	0.69	1.32	8.57
	Night	Above tropopause	−0.02	1.72	−0.01	1.87	0.01	1.02	–	–
		Below tropopause	0.13	1.4	0.02	1.46	0.08	0.66	1.62	8.32
Drift		Above tropopause	–	3.32	–	3.22	–	3.09	–	–
Descent	Day	Above tropopause	0.16	1.74	−0.02	1.9	0.9	1.14	–	–
		Below tropopause	0.14	1.65	0.01	1.7	0.42	0.75	−1.7	10.12
	Night	Above tropopause	0.16	1.73	0.03	1.84	0.21	1.06	–	–
		Below tropopause	0.15	1.67	0.05	1.67	0.04	0.73	0.5	10.47

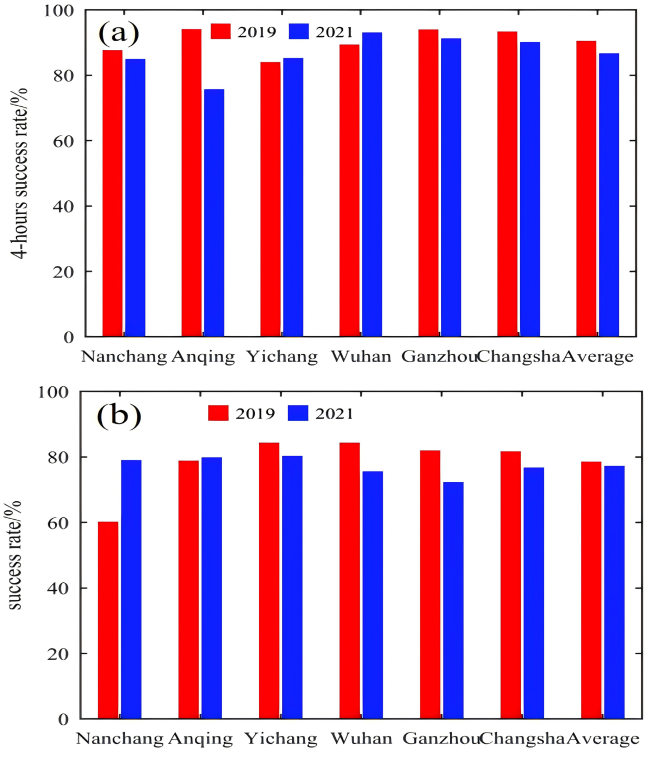

Figure 5. The field experiment in the middle and lower reaches of the Yangtze River Region (2019–2021): **(a)** drifting success rate; **(b)** 4 h drifting success rate.

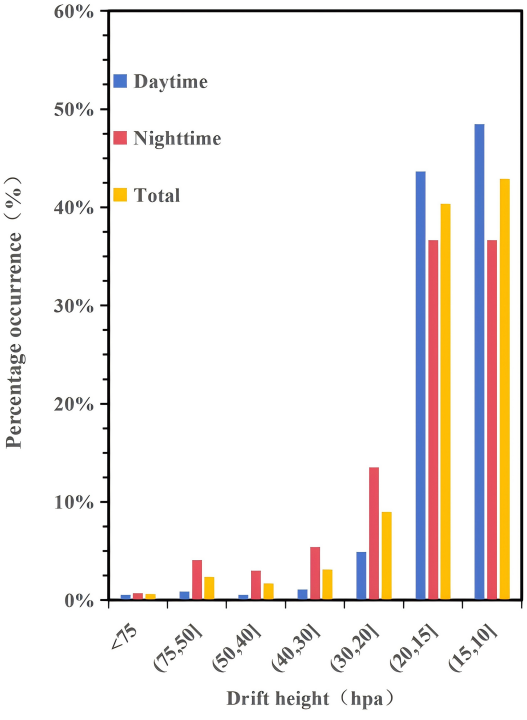

Figure 6. The drifting height of sounding-forecasting interactive network experiment (2021).

consistent with findings from other studies comparing high-resolution radiosonde data with reanalyses (Pauley and Ingleby, 2022; Ingleby, 2017). such differences are often attributed to representation errors arising from the inherent resolution mismatches.

A known warm bias, correlated with high initial descent rates (frequently $> 50\,m\,s^{-1}$), affects temperature measurements during the early descent (Ingleby et al., 2022). Consistent with operational practice, data from the initial high-descent-rate period in this study were filtered out prior to the comparison with reanalysis data presented. This quality control step mitigates the impact of this bias on the statistical results.

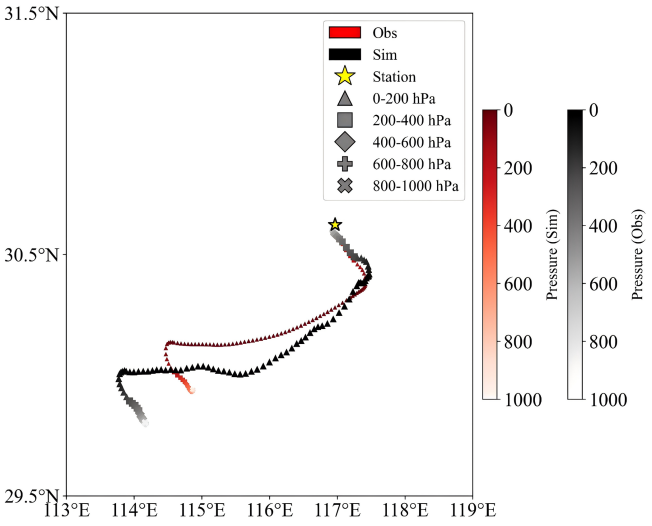

Figure 7. Schematic diagram of the observed (black) and simulated (red) trajectories. The yellow pentagram indicates the radiosonde station. The color of each point represents the corresponding pressure level. Distinct markers are used every 200 hPa to enhance visual differentiation.

5 Application of ADDRS in numerical forecasting techniques

5.1 A case study of weather analysis

Through long-term testing, the ADDRS have the potential to capture key information in convective system monitoring. From 8 to 9 July 2021, a strong convective weather event with a long duration and a large impact area occurred in the middle and lower reaches of the Yangtze River in China. Convection developed and moved to northern Jiangxi, northern Zhejiang, southern Anhui, and southern Jiangsu overnight on 8 July (Fig. 8). The drifting trajectories of ADDRS radiosondes were from west to east, which aligned with the movement and development direction of severe convection. The descent phase radiosondes of ADDRS provides effective monitoring and insights in tracking the occurrence of the convective system and the changes in the ambient field.

Figure 8 displays the trajectory data of the ADDRS and GTS12 radiosondes launched from the Wuhan Meteorological Station. On the night of 8 November, at 11:15 UTC, Wuhan was situated on the western flank of the main convective system. The ADDRS radiosonde was launched at this time from the station, followed by the GTS12 radiosonde at 12:00 UTC from the same location. During the ascent phase, the curve of the ADDRS radiosonde (Fig. 9b) exhibited a trend similar to that of the GTS12 (Fig. 9a). A comparison of the ascent-phase data revealed that the convective available potential energy (CAPE) values differed between the two instruments as convection developed. The GTS12 measured a CAPE of 1729.39 J kg^{-1} at 12:00 UTC, higher than the value of 1498.16 J kg^{-1} recorded by the ADDRS at 11:15 UTC.

Influenced by an upper-level westerly jet, the ADDRS sounding balloon drifted eastward toward the Wuhan. At 13:30 UTC, ADDRS conducted descent phase measurements (Fig. 9c). As shown in the layer curve, the CAPE value at 21:30 UTC decreased compared with that at 12:00 UTC, dropping to 646.0 J kg^{-1}, which was lower than the energy recorded at the Wuhan station. There is still a westerly jet stream with wind speed greater than 20 m s^{-1} beyond the upper-air of 500 hPa level. The east of Wuhan proximity to the main body of convection, the reduction in energy suggests intensive upward motion, leading to the reduction of effective potential energy and further develop of convective. Notably, the GTS12 radiosonde, launched from Wuhan, ceased data collection after the ascent phase, thus missing this crucial change. The descent phase of ADDRS demonstrates robust monitoring capabilities and holds significant implications, as it can timely captures environmental conditions favorable for convection onset and development, including wind patterns, effective potential energy, and humidity at downstream locations. These findings enable researchers to analyze changes in the upper-air field and the occurrence of catastrophic weather convective systems.

5.2 Applications in numerical weather prediction (NWP)

Unlike GTS12 radiosondes, the ADDRS radiosondes provide measurement data of both ascent and descent phase for numerical weather prediction (NWP), achieving a similar role to intensive sounding and providing more continuous, direct stratospheric measurement data (Zhang et al., 2025b, 2023). The Numerical Department of the China Meteorological Administration developed the key technology for ADDRS assimilation in the CMA-MESO 3DVar (three-dimensional variational mesoscale) (Zhuang et al., 2019) and CMA-GFS 4DVar systems (four-dimensional Variational Global Forecast System) (Wang et al., 2021b). To avoid the tangent linear and adjoint models, the four-dimensional ensemble forecast error is introduced into the CMA global data assimilation system, and the Hybrid-4DEnVar assimilation scheme is developed. The batch cycling forecast experiments and typhoon forecast experiments are conducted and compared with the 4DVar scheme (Gong et al., 2019; Wang et al., 2024a). Specifically, this includes observation operators that consider drift positions and vertical spacing methods, such as selecting the nearest radiosonde data from the model layer for assimilation. But the assimilation of drift-phase observations faces three primary challenges: first, the large warm bias in daytime temperature measurements, which significantly impacts assimilation quality; second, the high likelihood of correlated observation errors due to the very high horizontal resolution of the data ($\sim$ 100 m along-track) compared to the model grid. Current operational systems do not

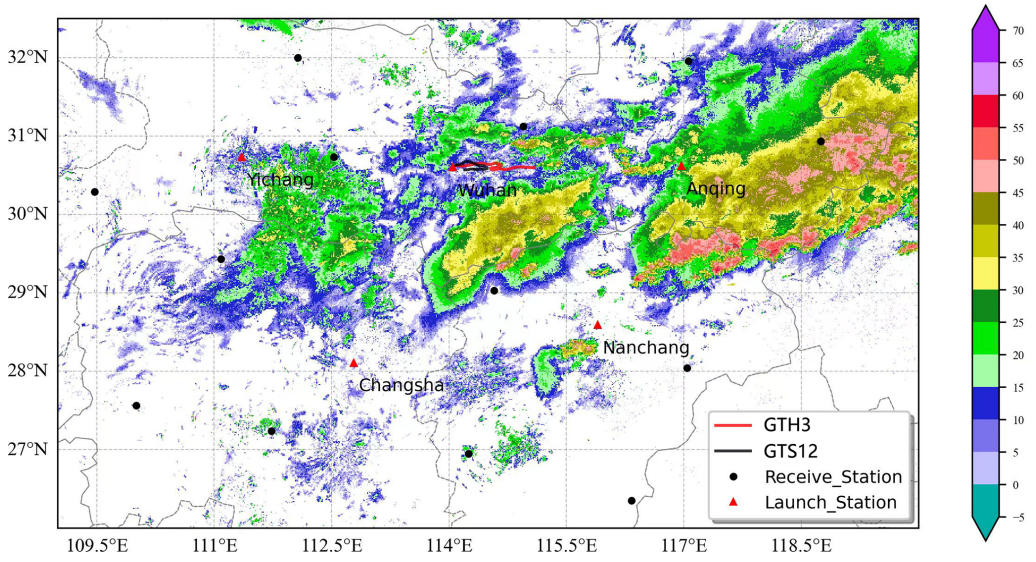

Figure 8. The trajectory for GTH3 and GTS12 radiosonde at the Wuhan station and radar reflectivity image at 12:00 UTC on 8 July 2021.

account for these error correlations, necessitating data thinning to improve assimilation effectiveness. Third, determining the optimal data segmentation or "batching" strategy for the continuous trajectory. Treating the entire drift phase as a single, vertical profile at an average location introduces significant representativeness error, as it ignores the sonde's substantial horizontal displacement. We employed the CMA-MESO system to conduct a measurement data assimilation in the ADDRS descent phase across six test stations in the middle and lower reaches of the Yangtze River from 1 to 31 July 2021. We set up the control test (CTL) as in the CMA-MESO system, and the observed data included traditional sounding data, ground reports, aircraft reports, cloud-guided wind, radar radial wind, GNSS occultation refractive index, and ground-based GNSS retrieval of the atmospheric whole-layer precipitation water. ADDRS data assimilation was added to the control CTL in the Down test.

The impact of the ADDRS descent phase measurement data on the precipitation forecast at CMA-MESO at 03:00, 06:00, 09:00, 15:00, 18:00, and 21:00 UTC (termed the warm start times) was evaluated. Compared to the TS (Threat Score), the ETS (Equitable Threat Score) imposes stricter penalty for false alarms and missed reports, making the scoring more equitable. The results of the one-month batch test indicate that assimilating ADDRS descent phase data improves precipitation forecasting skills, especially for heavy precipitation above a certain magnitude. Figure 10a and b illustrate the improvement rates in accumulated precipitation forecasting skills for the 0–12 and 12–24 h periods from the warm start time. Positive values indicate that the precipitation forecasting skills of the Down test are improved compared with those of the CTL test, while negative values indicate a decrease in forecasting skills for the Down test. The ETS scores for precipitation forecasts in the 0–12 h range at thresholds of 0.1, 1, and 50 mm increased slightly, averaging about 0.04 % (Fig. 10a). Due to the timeliness required for forecasting, the 12–24 h precipitation forecast is of particular interest to forecasters. As illustrated in Fig. 10b, the Down test demonstrated enhanced ETS scores for precipitation forecasts across all levels within the 12–24 h range, with an average increase of 0.7 % at the 50 mm threshold and a notable 2.2 % improvement specifically at this level. It is important to note that while these ETS improvements are consistent and positive, they have not yet reached conventional levels of statistical significance (e.g., $p < 0.05$) over the one-month test period, primarily due to the limited sample size of case studies. This underscores the preliminary yet promising nature of these findings.

In addition, we utilized CMA-MESO V5.1 to conduct Observing System Simulation Experiments (OSSE) under the ADDRS network nationwide. The results indicate that once the ADDRS network observation is implemented, the national precipitation forecast skills of the CMA-MESO fast cycle assimilation forecast system at warm startup time can improve by 2 %–5 %. The applications of ADDRS high-resolution data were quantitatively evaluated using a numerical model (Wang et al., 2023). After the application of ADDRS data in CMA-GFS 4DVar assimilation, the temperature analysis error at 06:00 and 18:00 UTC was reduced by more than 2 % and the average prediction skill of the CMA-MESO accumulated precipitation results for the 12–36 h period improved by 1 % (Wang et al., 2024b).

5.3 Applications in targeted observations

Targeted observations have sometimes been a frontier field in atmospheric science. They represent a possible method to address the shortcomings of conventional observation sys-

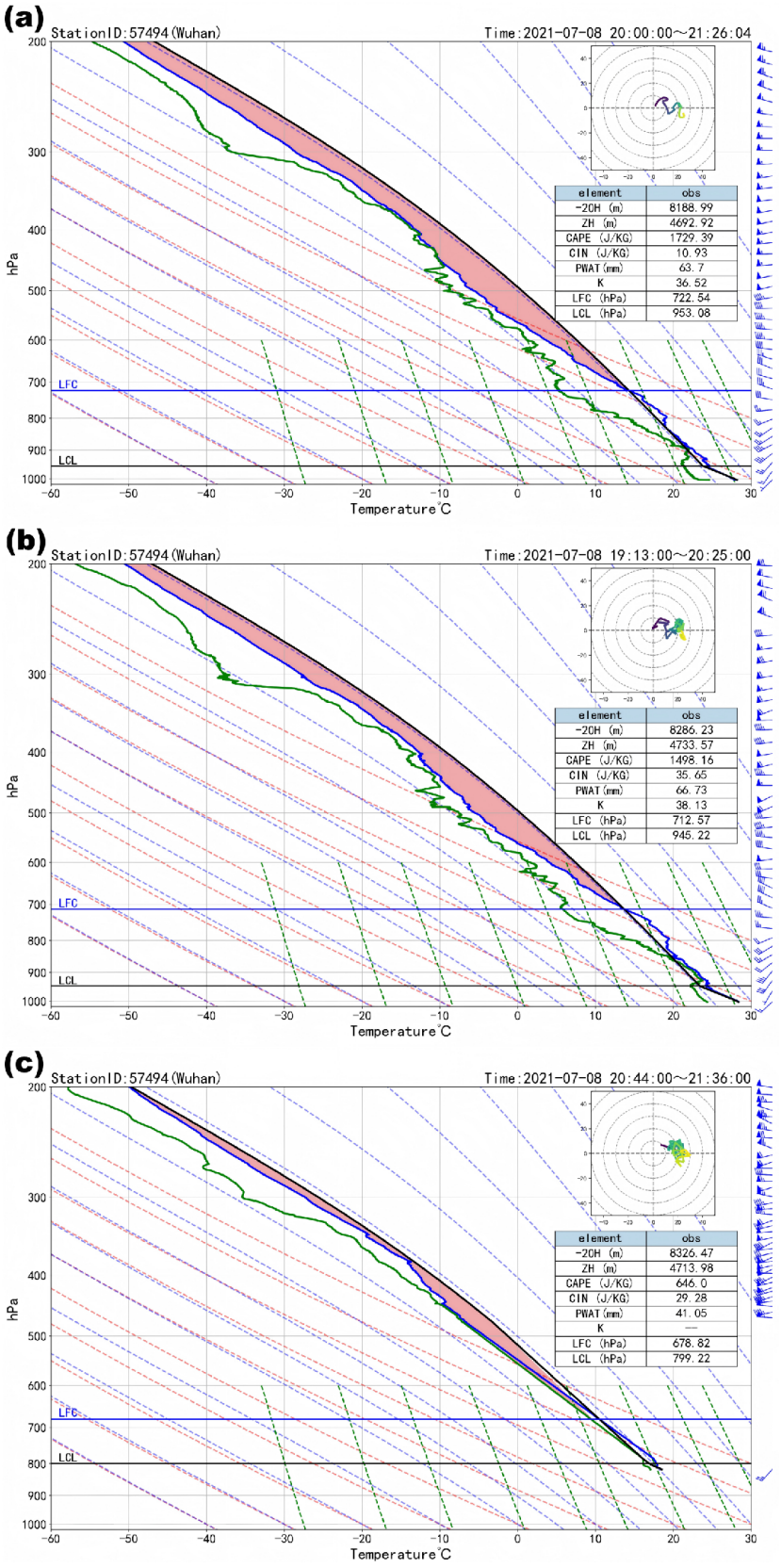

Figure 9. Comparison of ADDRS and GTS12 radiosonde T-logP at the Wuhan station: **(a)** GTS12 radiosonde; **(b)** ascent phase of ADDRS radiosonde; **(c)** descent phase of ADDRS radiosonde.

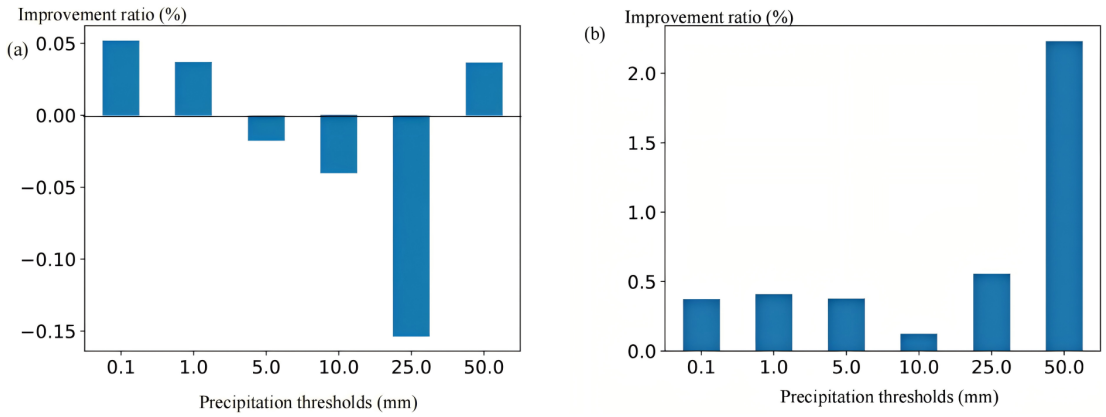

Figure 10. Improvement rates of cumulative precipitation thresholds (mm) predictions for 0–12 h **(a)** and 12–24 h **(b)** in the Down test compared to the control test.

tems in monitoring extreme weather events. Furthermore, they sometimes enhance the initial field quality and forecast accuracy of numerical models (Majumdar, 2016). With its capacity for "ADD" measurement, the ADDRS has the potential to conduct targeted observations in uninhabited areas, rarely observed regions, and during specific extreme weather events. However, since the ADDRS lacks a steering system, accurate trajectory prediction is essential for utilizing the descent phase for vertical measurements in these locations. This requires careful consideration of appropriate drift height, launch time, and launch location, allowing the ADDRS sounding to be carried to the target observation area by the ambient wind field.

In this context, a trajectory prediction and selection method based on high-resolution numerical weather prediction technology has been proposed for ADDRS (Wang et al., 2021a). Additionally, Majumdar (2016) highlights that advancements in numerical weather prediction (NWP) systems – such as improved data assimilation techniques and enhanced model resolution – have reduced the marginal contributions of individual observing systems. Furthermore, the evaluation of targeted observations is constrained by factors including flow-dependent conditions, limited sample sizes, and inconsistencies in verification metrics. Therefore, cost-effective strategies for targeted observations necessitate exploration through multi-agency coordinated observing system experiments, such as FSO studies (Magnusson et al., 2025).

5.3.1 Trajectory prediction method and software system

The issues of low temporal resolution and prediction accuracy associated with the linear extrapolation method used in balloon trajectory prediction (Brown et al., 2024). The balloon trajectory equation is directly embedded into a high-resolution numerical weather model system that utilizes a model atmospheric environment with high temporal resolution (1–10 s) and high spatial resolution (1–3 km). This approach enables precise simulation of vertical velocity during the ADDRS descent phase (Fig. 11a), enhancing the accuracy of ADDRS trajectory prediction and the simulation of descent velocity. The average prediction error for a 6 h trajectory is less than 40 km (Fig. 11b).

5.3.2 Trajectory selection method based on the collection idea

To observe the ADDRS in the target observation area, we proposed a method of elevation selection based on ensemble forecasting, considering the characteristics of the atmospheric wind field as it varies with altitude. The main idea of this method is to predict the trajectories of all ADDRS stations at different drifting heights and select the heights closest to the target observation area. The details are as follows:

1. Identify the positions and launch time: Given the positions $\mathrm{Sm}(x_m, y_m, z_m)$ of M ADDRS launch stations and the launch time t_r.

2. Select safe drift heights: Choose N safe drift heights $h_1, h_2, \ldots, h_n$, that comply with civil aviation safety regulations as flat drift heights.

3. Trajectory prediction: Utilize the trajectory prediction system to predict the ADDRS trajectories under the above conditions within 12 h, resulting in $\mathrm{Tnm}(x, y, z, t)$ for N trajectories at each of the M launch stations.

4. Calculate closest trajectory: From the $M \times N$ trajectories obtained in step 3, calculate the trajectory closest to the target observation point. When the distance is less than the predetermined standard distance L_C that can meet the requirements, the releasing ADDRS station and the drifting height H_s are selected, and the time

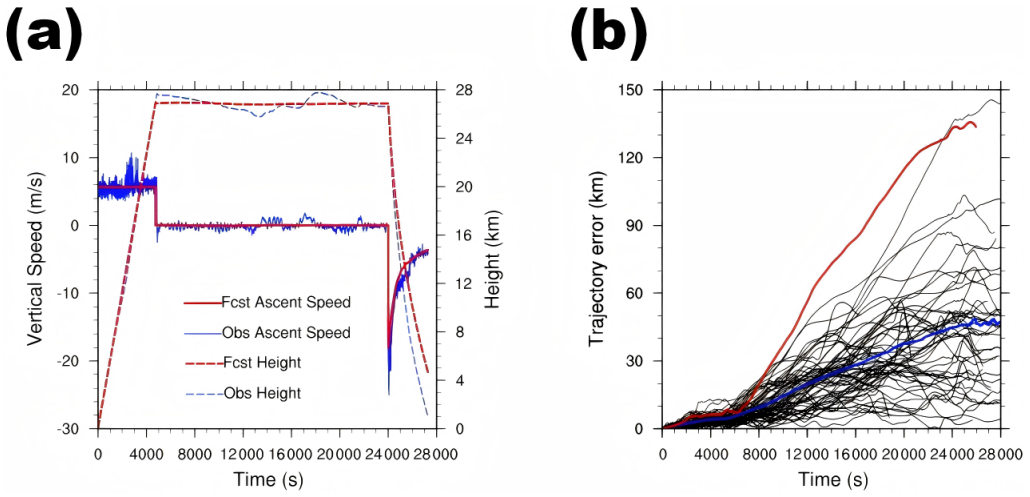

Figure 11. **(a)** Comparison of simulated (red line) and observed (blue line) vertical speeds of ADDRS radiosonde data during the descent phase at the Anqing station at 11:17 UTC on 20 June 2018. **(b)** Deviations of 63 pairs of simulated ADDRS trajectories versus observed trajectories (black line), with the average deviation indicated by the blue line and the largest forecast deviation shown by the red line.

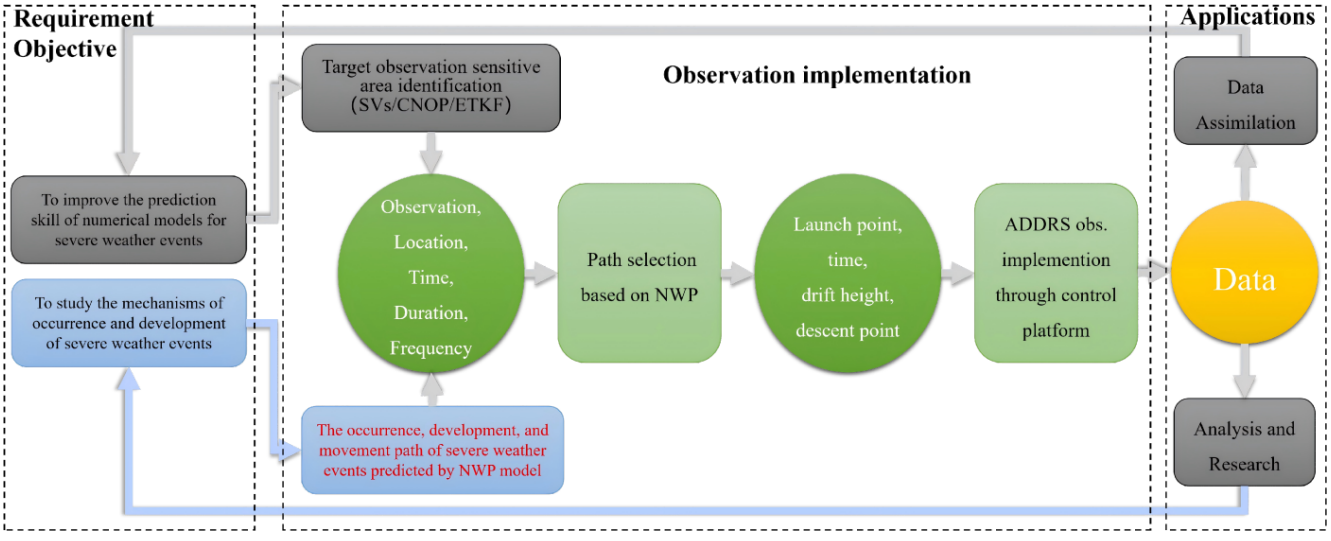

Figure 12. Technical route for targeted observations of typhoons and other severe weather using ADDRS and CMA-MESO models.

nearest to the target area is taken as the descent time t_s. If no suitable drift height meets the conditions, the trajectory selection fails.

5. Implement target observation: Input the information regarding the ADDRS balloon launch station, drift height, and descent time determined in step 4 into the ADDRS operation command system to execute the target observation.

5.3.3 Targeted observations experiment of Typhoon

The ADDRS research team proposed a "full chain" implementation for target observation using ADDRS (Fig. 12). This implementation plan, designed to provide technical support for ADDRS applications in disaster weather monitoring, forecasting, and mechanism research, encompasses three primary phases. Initially, the requirements for target observation are established. These requirements fall into two categories: one focusing on specific disaster weather events and the other on sensitive areas to improve future numerical prediction skills. The target observation area is then determined based on the type of demand. For the first category, the specific location of anticipated disaster weather is identified through numerical prediction results. For the second category, the target observation location is determined using CMA-GFS singular vector technology.

Subsequently, the trajectory selection system is invoked to ascertain the ADDRS launch station, drift height, launch

and subsequent descent phases time, and other relevant information. This information is then transmitted to the operation command system of ADDRS to guide the stations in implementing ADDRS measurements. Ultimately, the ADDRS target observation data is distributed to users for application and evaluation.

According to the implementation plan for ADDRS target observation (Zhang et al., 2021a; Liu et al., 2022a), we made a preliminary attempt to conduct a target observation experiment on Typhoon 2309 "SAOLA" (Lau et al., 2024) formed at 00:00 UTC on 28 August 2023. By 00:00 UTC on 1 September, it was expected that "SAOLA" would make landfall near Guangdong on 2 September. Therefore forecasters sought profiles of the inner structure of Typhoon "SAOLA". Note also the importance of the steering flow and use of satellite data to analyse the wider environment of tropical storms (Magnusson et al, 2025). Using the typhoon trajectory predicted by CMA-GFS, we pinpointed the typhoon's position for 12:00 pm UTC on 2 September post-landfall. The ADDRS trajectory selection system was then engaged to ascertain the balloon launch station and drift height that could reach or come closest to the typhoon area, ranging from the minimum navigation safety height of 21 to 29 km. We set ten different drift levels at 1 km intervals, with trajectory predictions and simulations conducted from four radiosonde observations stations in Guangdong. Yangjiang radiosonde observations station in Guangdong was ultimately chosen for the launch, scheduled for 06:00 UTC on 2 September 2023, with a drift level of 25 km.

We calculated the required hydrogen capacity for the dual-mode balloon, and the "ADD" subsystem was prepared to be deployed by radiosonde observations station personnel. When the radiosonde reached the core area of "SAOLA" the radiosonde dispatched commands to the "SAOLA" controller via control command transmission equipment, successfully observing the descent phase 80 km from the center of Typhoon "SAOLA" The obtained ADDRS data was subsequently assimilated into the CMA_MESO 3DVar system. Test results indicated that after assimilating the data from the ADDRS descent phase, the forecast error for the typhoon trajectory reported since 06:00 UTC on 2 September 2023, was reduced. Specifically, the typhoon trajectory error at 02:18 UTC was reduced from 62.7 to 35 km in the control test ,marking an improvement of 44.18 %. Additionally, precipitation forecasting techniques exhibited improvements: from 0.25 to 0.30 in the 10 mm scale, from 0.30 to 0.55 in the 25 mm scale, and from 0.45 to 0.70 in the 50 mm scale. These results effectively demonstrate the potential of ADDRS in target observation and numerical assimilation applications (Fig. 13). It is worth noting that the initial use of ADDRS for target observation served as a foundational attempt, paving the way for future ADDRS operations and maximizing its utility (Wen et al., 2025).

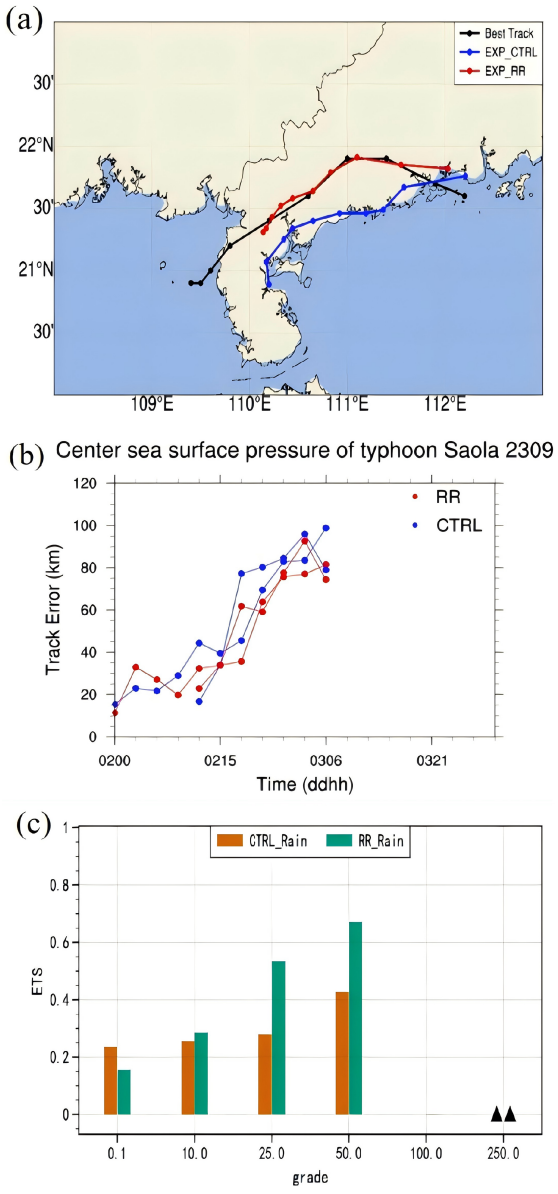

Figure 13. 2 September 2023 00:00 UTC to 3 September 2023 06:00 UTC: **(a)** Control test (blue), ADDRS data assimilation impact test (red), and optimal trajectory of Typhoon "Saola" (black). **(b)** Comparison of sea level pressure at the central point of Typhoon "Saola" between the control test (blue) and the ADDRS data assimilation impact test (red). **(c)** ETS scores for 0–24 h of precipitation forecast from control trials (orange) and ADDRS data assimilation impact trials (green).

6 Summary

ADDRS represents a possible next-generation approach for upper air sounding, adding substantial flexibility compared to currently operational sounding systems, We developed a multi-station real-time reception system utilizing "Internet cloud + Instruments terminal" technology. Additionally, up-

link commands can be sent from the ground to facilitate descent measurements in designated areas and targeted observations in weather-sensitive regions. Following over five years of extensive research and numerous field tests, the instruments, software, and operation guidelines of the system have achieved a refined level of maturity. Starting 1 January 2024, ADDRS already undergo operation experiments at four radiosonde observations stations in Guangdong, China. Since July 2024, a planned trial at 127 CMA radiosonde observation stations aims to achieve full operation capability by 2026. The positive impact of ADDRS data assimilation demonstrated here, even if not yet statistically significant over a one-month sample, has shown considerable applicable promise. ADDRS is a situational profiling technique that offers cost-effective upper-air measurements, making it suitable for widespread application in WMO's pre-operational sounding (e.g., RA II-18-I-DP-2). However, challenges remain, such as improving the drift success rate, enhancing relevant technologies, and fully leveraging the potential of continuous measurement data during the drift phase.

Data availability. The ADDRS research team previously hosted data on platform (https://www.r7tec.com/html/report/20040875-1.htm, last access: 17 May 2026).

More research data acquisition requires formal request to the corresponding authors: Xiaozhong Cao (Dr. Cao, caoxzh@cma.gov.cn); and Peng Zhang (Dr. Zhang, zhangp@cma.gov.cn).

Author contributions. XC, PZ, conceptualization and methodology; QG and HL designed the experiments and writing-original draft, supervision; JW, DX, JD, ZS, SL carried out the experiments; HL, QG, JW, RY, analyzed the experimental results; HL, QG, GJ, SC, AH revised the paper and participated in the discussion.

Competing interests. The contact author has declared that none of the authors has any competing interests.

Disclaimer. Publisher's note: Copernicus Publications remains neutral with regard to jurisdictional claims made in the text, published maps, institutional affiliations, or any other geographical representation in this paper. The authors bear the ultimate responsibility for providing appropriate place names. Views expressed in the text are those of the authors and do not necessarily reflect the views of the publisher.

Acknowledgements. The authors are thankful to the editor and all anonymous reviewers for their help in im-proving this manuscript.

This research was supported by the National Key Research and Development Program of China (grant no. 2018YFC1506200), the Innovation Team of the China Meteorological Administration (grant no. CMA2023QN11), and the Special Program for Innovation and Development of the China Meteorological Administration (grant no. CXFZ2023J064).

We thank Mr. Jiachun Yang and Mrs. Jie Xu to support the performance parameter of GTH3 radiosonde. And Dr. Lebao Yao, Mr. Yiwei Tao, Mr. Fei Xie and Mrs. Yonghong Niu to support for technical assistance with data analysis. We also extend our gratitude to the Xilinhot GRUAN site and other 17 upper-air meteorological stations for supplying the radiosonde data used in this study.

Financial support. This research has been supported by the National Natural Science Foundation of China, Key Programme (grant no. U2442214).

Review statement. This paper was edited by Chunlüe Zhou and reviewed by Bruce Ingleby and two anonymous referees.

References

Anand, D., Kumar, B. S., and Ojha, D.: TIFR Zero-Pressure balloon program crosses a milestone, Curr. Sci., 120, 1672–1678, https://doi.org/10.18520/cs/v120/i11/1672-1678, 2021.

Bauer, P., Radnóti, G., Healy, S., and Cardinali, C.: GNSS Radio Occultation Constellation Observing System Experiments, Mon. Wea. Rev., 142, 555–572, https://doi.org/10.1175/MWR-D-13-00130.1, 2014.

Bauer, P., Thorpe, A., and Brunet, G.: The quiet revolution of numerical weather prediction, Nature, 525, 47–55, https://doi.org/10.1038/nature14956, 2015.

Bormann, N., Lawrence, H., and Farnan, J.: Global observing system experiments in the ECMWF assimilation system, ECMWF Technical Memorandum, 839, 24, https://doi.org/10.21957/sr184iyz, 2019.

Brown, D., Linz, M., and Leidich, J.: Seasonal and geographic viability of high altitude balloon navigation, Sci. Rep., 14, 21861, https://doi.org/10.1038/s41598-024-71445-9, 2024.

Cao, X. Z., Guo, Q. Y., and Yang, R. K.: Research of rising and falling twice sounding based on long-time interval of flat-floating, Chinese Journal of Scientific Instrument, 40, 198–204, http://yqyb.etmchina.com/yqyb/article/abstract/20190223?st=search (last access: 17 May 2026), 2019 (in Chinese).

Cao, X. Z., Xia, Y. C., Luo, H. W., Liu, L. H., Liu, Y. F., Liu, Z. Y., Li, X., Guo, R., and Guo, Q. Y.: Technical development and prospect of meteorological sounding measurement, J. Adv. Meteorol. Sci. Technol., 12, 27–36, https://doi.org/10.3969/j.issn.2095-1973.2022.05.005, 2022 (in Chinese).

Cohn, S., Hock, T., Cocquerez, P., and Cole, H.: Driftsondes: providing in situ long-duration dropsonde observations over remote regions, Amer. Meteor. Soc., 94, 1661–1674, https://doi.org/10.1175/BAMS-D-12-00075.1, 2013.

DuBois, J. L., Multhauf, R. P., and Ziegler, C. A.: Invention and Development of the Radiosonde with a Catalog of Upper-Atmospheric Telemetering Probes in the National Museum of American History, Smithsonian Institution, Smithsonian Studies in History and Technology, 53, 1–78, https://doi.org/10.5479/si.00810258.53.1, 2002.

Fujiwara, M., Sun, B., Reale, A., Cimini, D., Larosa, S., Borg, L., von Rohden, C., Sommer, M., Dirksen, R., Maturilli, M., Vömel, H., Kivi, R., Ingleby, B., Kramer, R. J., Demoz, B., Madonna, F., Carminati, F., Lewis, O., Candy, B., Thomas, C., Edwards, D., Noersomadi, Shimizu, K., and Thorne, P.: Justification for high-ascent attainment for balloon radiosonde soundings at GRUAN and other sites, Atmos. Meas. Tech., 18, 2919–2955, https://doi.org/10.5194/amt-18-2919-2025, 2025.

Gallice, A., Wienhold, F. G., Hoyle, C. R., Immler, F., and Peter, T.: Modeling the ascent of sounding balloons: derivation of the vertical air motion, Atmos. Meas. Tech., 4, 2235–2253, https://doi.org/10.5194/amt-4-2235-2011, 2011.

Goff, J. A.: Saturation pressure of water on the new Kelvin temperature scale, Transactions of the American Society of Heating and Ventilating Engineers, 63, 347–354, 1957.

Gong, J. D., Liu, Y. Z., and Zhang, L.: A study of simplification and linearization of the NSAS deep convection cumulus parameterization scheme for 4D-Var, Acta Meteorol. Sin., 77, 595–616, https://doi.org/10.11676/qxxb2019.048, 2019 (in Chinese).

Gong, N., Liu, Y. F., Ren, J., Wu, Q., and Hu, H. L.: A Novel Adaptive Resource Allocation Framework for Sounding Networks, 2021 the 11th International Workshop on Computer Science and Engineering (WCSE 2021), 276–283, https://doi.org/10.18178/wcse.2021.06.040, 2021.

Guo, Q. Y., Yang, J. C., Yang, R. K., Qian, Y., and Cao, X. Z.: Evaluation of wind performance of domestic Beidou dropsonde of ball-loading, J. Nanjing Univ. Inf. Eng. Nat. Sci. Ed., 10, 12, https://doi.org/10.13878/j.cnki.jnuist.2018.05.014, 2018 (in Chinese).

Haig, T. O. and Lally, V. E.: Meteorological Sounding Systems, B. Am. Meteorol. Soc., 39, 401–409, https://doi.org/10.1175/1520-0477-39.8.401, 1958.

He, Y., Zhu, X., Sheng, Z., and He, M.: Identification of stratospheric disturbance information in China based on the round-trip intelligent sounding system, Atmos. Chem. Phys., 24, 3839–3856, https://doi.org/10.5194/acp-24-3839-2024, 2024.

Hersbach, H., Bell, B., Berrisford, P., Hirahara, S., Horányi, A., Muñoz-Sabater, J., Nicolas, J., Peubey, C., Radu, R., Schepers, D., Simmons, A., Soci, C., Abdalla, S., Abellan, X., Balsamo, G., Bechtold, P., Biavati, G., Bidlot, J., Bonavita, M., De Chiara, G., Dahlgren, P., Dee, D., Diamantakis, M., Dragani, R., Flemming, J., Forbes, R., Fuentes, M., Geer, A., Haimberger, L., Healy, S., Hogan, R. J., Hólm, É., Janisková, M., Keeley, S., Laloyaux, P., Lopez, P., Lupu, C., Radnoti, G., de Rosnay, P., Rozum, I., Vamborg, F., Villaume, S., and Thépaut, J.-N.: The ERA5 global reanalysis, Q. J. R. Meteorolog. Soc., https://doi.org/10.1002/qj.3803, 2020.

Hertzog, A., Plougonven, R., and the Stratéole-2: Strateole-2: High-resolution observations of the tropical tropopause layer with long-duration balloons, EGU General Assembly 2021, online, 19–30 April 2021, EGU21-7109, https://doi.org/10.5194/egusphere-egu21-7109, 2021

Ingleby, B.: An assessment of different radiosonde types 2015/2016, ECMWF Technical Memorandum No. 807, 69 pp., https://doi.org/10.21957/0nje0wpsa, 2017.

Ingleby, B., Pauley, P., Kats, A., Ator, J., and Weedon, R.: Progress toward high-resolution, real-time radiosonde reports, B. Am. Meteorol. Soc., 97, 2149–2161, https://doi.org/10.1175/BAMS-D-15-00169.1, 2016a.

Ingleby, B., Rodwell, M., and Isaksen, L.: Global radiosonde network under pressure, ECMWF Newsletter No. 149 – Autumn 2016, 25–30, https://docslib.org/doc/2149971/global-radiosonde-network-under-pressure (last access: 17 May 2026), 2016b.

Ingleby, B., Motl, M., Marlton, G., Edwards, D., Sommer, M., von Rohden, C., Vömel, H., and Jauhiainen, H.: On the quality of RS41 radiosonde descent data, Atmos. Meas. Tech., 15, 165–183, https://doi.org/10.5194/amt-15-165-2022, 2022.

Johnson, A., Wang, X., Hutchinson, T., and Creus-Costa, J.: Impact of WindBorne observation assimilation on prediction of a TPV merger case from THINICE, J. Geophys. Res.-Atmos., 129, e2024JD041395, https://doi.org/10.1029/2024JD041395, 2024.

Lau, D. S., Chan, W. S., Wong, Y. C., Lam, C. C., and Chan, P. W.: Hindcast Insights from Storm Surge Forecasting of Super Typhoon Saola (2309) in Hong Kong with the Sea, Lake and Overland Surges from Hurricanes Model, Atmos., 15, 17, https://doi.org/10.3390/atmos15010017, 2024.

Liu, L. H., Han, Y., Xia, Y. C., Guo, Q. Y., Gao, W., and Guo, J. P.: Investigation of Atmospheric Dynamic and Thermodynamic Structures of Typhoon Sinlaku (2020) from High-Resolution Dropsonde and Two-Way Rawinsonde Measurements, Remote Sens., 14, 2704, https://doi.org/10.3390/rs14112704, 2022a.

Liu, S. J., Yang, R. K., Cao, X. Z., Guo, Q. Y., Cheng, K. Q., Kan, Z. P., and Wang, J. C.: Analysis and Numerical Experiment of the Horizontal Drift Round-trip Sounding Balloon's Dynamic and Thermal Process in the Adjacent Space, Chin. J. Atmos. Sci., 46, 788–804, https://doi.org/10.3878/j.issn.1006-9895.2110.20252, 2022b (in Chinese).

Liu, Y. F., Zhou, Y. Y., Du, J. P., Liu, D., Ren, J., Chen, Y. H., Zhang, F., and Chen, J. P.: RTP-GRU: Radiosonde Trajectory Prediction Model Based on GRU, in: Advances in Intelligent Systems and Computing (AISC, volume 1274), 24, 543–550, https://doi.org/10.1007/978-981-15-8462-6_61, 2021.

Magnusson, L., Majumdar, S. J., Dahoui, M. L., Bormann, N., Bonavita, M., Browne, P. A., Brown, A. R., De Chiara, G., Duncan, D. I., English, S., Geer, A. J., Healy, S., Ingleby, B., McNally, A. P., Pappenberger, F., Prates, F., Rabier, F., de Rosnay, P., Rennie, M. P., and Warrick, F.: The role of observations in ECMWF tropical cyclone initialisation and forecasting, Q. J. R. Meteorolog. Soc., 151, e4924, https://doi.org/10.1002/qj.4924, 2025.

Majumdar, S. J.: A review of targeted observations, B. Am. Meteorol. Soc., 97, 2287–2303, https://doi.org/10.1175/BAMS-D-14-00259.1, 2016.

Marlton, G. J., Harrison, R. G., Nicoll, K. A., and Williams, P. D.: A balloon-borne accelerometer technique for measuring atmospheric turbulence, Rev. Sci. Instrum., 86, 016109, https://doi.org/10.1063/1.4905529, 2015.

Pauley, P. M. and Ingleby, B.: Assimilation of in-situ observations, in: Data Assimilation for Atmospheric, Oceanic and Hydrologic Applications, Vol. IV, edited by: Park, S. K. and Xu, L., Springer, Cham, 293–371, https://doi.org/10.1007/978-3-030-77722-7_12, 2022.

Pettifer, R. E.: From Observations to Forecasts – Part 2. The development of in situ upper air measurements, Weather, 64, https://doi.org/10.1002/wea.484, 2009.

Raman, M. R., Ratnam, M. V., Rajeevan, M., Rao, V. V. M. J., and Rao, S. V. B.: Intriguing Aspects of the Monsoon Low-

Level Jet over Peninsular India Revealed by High-Resolution GPS Radiosonde measurements, J. Atmos. Sci., 68, 1413–1423, https://doi.org/10.1175/2011JAS3611.1, 2011.

Seidel, D. J., Berger, F. H., Diamond, H. J., Dykema, J., Goodrich, D., Immler, F., Murray, W., Peterson, T., Sisterson, D., Sommer, M., Thorne, P., Vomel, H., and Wang, J.: Reference Upper-Air Observations for Climate: Rationale, Progress, and Plans, B. Am. Meteorol. Soc., 90, 361–369, https://doi.org/10.1175/2008BAMS2540.1, 2009.

Shen, Z. P., Pan, X. Z., and Yi, Y. L.: Preparation and properties of modified nano-clay/natural latex composites, J. Rubber Ind., 67, 4, https://doi.org/10.12136/j.issn.1000-890X.2020.08.0580, 2020 (in Chinese).

Venkat Ratnam, M., Pravallika, N., Ravindra Babu, S., Basha, G., Pramitha, M., and Krishna Murthy, B. V.: Assessment of GPS radiosonde descent data, Atmos. Meas. Tech., 7, 1011–1025, https://doi.org/10.5194/amt-7-1011-2014, 2014.

Vernier, H., Rastogi, N., Liu, H., Pandit, A. K., Bedka, K., Patel, A., Ratnam, M. V., Kumar, B. S., Zhang, B., Gadhavi, H., Wienhold, F., Berthet, G., and Vernier, J.-P.: Exploring the inorganic composition of the Asian Tropopause Aerosol Layer using medium-duration balloon flights, Atmos. Chem. Phys., 22, 12675–12694, https://doi.org/10.5194/acp-22-12675-2022, 2022.

Vernier, J.-P., Fairlie, T. D., Deshler, T., Ratnam, M. V., Gadhavi, H., Kumar, B. S., Natarajan, M., Pandit, A. K., Raj, S. T. A., Kumar, A. H., Jayaraman, A., Singh, A. K., Rastogi, N., Sinha, P. R., Kumar, S., Tiwari, S., Wegner, T., Baker, N., Vignelles, D., Stenchikov, G., Shevchenko, I., Smith, J., Bedka, K., Kesarkar, A., Singh, V., Bhate, J., Ravikiran, V., Rao, M. D., Ravindrababu, S., Patel, A., Vernier, H., Wienhold, F. G., Liu, H., Knepp, T. N., Thomason, L., Crawford, J., Ziemba, L., Moore, J., Crumeeyrolle, S., Williamson, M., Berthet, G., Jégou, F., and Renard, J. B.: BATAL: The Balloon Measurement Campaigns of the Asian Tropopause Aerosol Layer, B. Am. Meteorol. Soc., 99, 955–973, https://doi.org/10.1175/BAMS-D-17-0014.1, 2018.

Wang, D., Wang, J. C., Tian, W. H., and Guo, Q. Y.: Quality control and uncertainty analysis of Round-trip drifting sounding system data, Chinese J. Atmos. Sci., 44, 20, https://doi.org/10.3878/j.issn.1006-9895.1912.19203, 2020 (in Chinese).

Wang, F., Gong, J. D., Wang, R. C., and Chen, Y. D.: A methodological study of the CMA global hybrid four-dimensional variational data assimilation system, Acta Meteorol. Sin., 82, 709–720, https://doi.org/10.11676/qxxb2024.20230140, 2024a (in Chinese).

Wang, J. C., Wang, D., Yang, R. K., Cao, X. Z., and Guo, Q. Y.: A Return Radiosonde Trajectory Forecast Method and Its Preliminary Evaluation Based on High Resolution Numerical Weather Prediction Model, Chinese J. Atmos Sci., 45, 651–663, https://www.iapjournals.ac.cn/dqkx/cn/article/Y2021/I3/651 (last access: 17 May 2026), 2021a.

Wang, J. C., Wang, D., Wang, R. W., Tan, J., and Rong, N.: Assimilation of Round-Trip Horizontal Drift Radiosonde Data in CMA-MESO 3DVar and Its Impact on Model Forecast, Meteorol. Mon., 50, 50–60, https://doi.org/10.7519/j.issn.1000-0526.2023.110501, 2024b (in Chinese).

Wang, J. H., Young, K., Hock, T., Lauritsen, D., Behringer, D., Black, M., Black, P. G., Franklin, J., Halverson, J., Molinari, J., Nguyen, L., Reale, T., Smith, J., Sun, B., Wang, Q., and Zhang, J. A.: A long-term, high-quality, high-vertical resolution GPS dropsonde data set for hurricane and other studies, B. Am. Meteorol. Soc., 96, 961–973, https://doi.org/10.1175/BAMS-D-13-00203.1, 2015.

Wang, R. W., Han, W., Tian, W. H., and Gong, J. D.: Blacklist Design of AMDAR Temperature Data and Their Application in the CMA-GFS, J. Trop. Meteorol., 27, 368–377, https://doi.org/10.46267/j.1006-8775.2021.032, 2021b.

Wang, R. W., Wang, J. C., Wang, D., Tao, Y. W., and Tian, W. H.: Study on the Influence of Return Sounding Observation System Based on CMA-MESO, Meteorol. Mon., 49, 52–61, https://doi.org/10.7519/j.issn.1000-0526.2022.032601, 2023 (in Chinese).

Wen, Q. S., Zhang, X. F., Hu, S., Zhao, P. T., Zhong, S. X., Liu, Z. Y., Zhao, Z. K., Liang, J. H., Dai, G. F., Zhang, C. Z., Li, M. J., and Huang, L.: Collaborative assimilation experiment of Beidou radiosonde and drone-dropped radiosonde based on CMA-TRAMS, Atmos. Ocean. Sci. Lett., 18, https://doi.org/10.1016/j.aosl.2024.100555, 2025.

WMO (World Meteorological Organization): The gaps in the Global Basic Observing Network (GBON), SOFF Series No. 2, p. 4, https://library.wmo.int/idurl/4/57174 (last access: 17 May 2026), 2020.

WMO (World Meteorological Organization): 8th WMO Workshop on the Impact of Various Observing Systems on Numerical Weather Prediction and Earth System Prediction, Norrköping, Sweden, https://community.wmo.int/en/meetings/8th-wmo-impact-workshop-home (last access: 17 May 2026), 2024a.

WMO (World Meteorological Organization): Instruments and Observing Methods Report No. 143: Report of WMO's 2022 Upper-Air Instruments Intercomparison Campaign, Geneva, 22 pp., https://library.wmo.int/idurl/4/68808 (last access: 17 May 2026), 2024b.

WMO (World Meteorological Organization): Guide to Meteorological Instruments and Methods of Observation, Volume III – Observing Systems, WMO-No. 8, 2025 edition, Geneva, 464 pp., https://doi.org/10.59327/WMO/CIMO/3, 2025.

Xu, H. F., Guo, Q. Y., Liu, Y. Z., Lin, T. N., Ma, P. Q., and Dong, F. Z.: Key factors influencing drift success rate of new-type meteorological balloons, Journal of Applied Meteorological Science, 36, 427–440, https://doi.org/10.11898/1001-7313.20250404, 2025 (in Chinese).

Yang, C. Y., Guo, Q. Y., Cao, X. Z., and Zhang, W.: Analysis of gravity wave characteristics in the lower stratosphere based on new round-trip radiosonde, Acta Meteorol. Sin., 79, 150–167, https://doi.org/10.11676/qxxb2021.008, 2021 (in Chinese).

Yang, C. Y., Cao, X. Z., Guo, Q. Y., and Yuan, Y.: Feature Extraction and Analysis of Atmospheric Turbulence Based on New Round-Trip Radiosonde, Chinese J. Atmos. Sci., 47, 1967–1982, https://www.iapjournals.ac.cn/dqkx/article/exportPdf?id=bbe5bcd7-643c-4986-b364-2260622abbda (last access: 17 May 2026), 2023 (in Chinese).

Yang, J. C., Wang, Y. M., Li Q. J., Jia K. B., and Liu, P. Y.: Research on error prediction technology of radiosonde temperature sensor, Journal of Electronic Measurement and Instrumentation, 35, 24–26, https://doi.org/10.13382/j.jemi.B2104288, 2022 (in Chinese).

Yang, R. K., Wang, Y., and Liu, Q. Q.: Dynamic Performance Analysis of Sounding temperature sensor, Sci. Technol. Eng., 4, 57–60, https://doi.org/10.3969/j.issn.1671-1815.2014.04.012, 2014 (in Chinese).

Yao, L. B., Shen, D., Sun, X., Wang, D. H., Cao, X. Z., Wang, J. C., Wang, D., Zhang, C. Y., and Guo, Q. Y.: Ascent-drift-descent radiosonde system: Field experiments and data quality assessment, Atmos. Res., 329, 108489, https://doi.org/10.1016/j.atmosres.2025.108489, 2026.

Zhang, C. Z., Huang, Y. Y., Liang, J. H., and Xu, H. F.: Application Experiment of Assimilating Beidou Satellite Navigation Round-Trip Sounding Data Observed in Guangdong Province Using CMA-GD Model, J. Trop. Meteorol., 41, 16–25, https://doi.org/10.16032/j.issn.1004-4965.2025.001, 2025a (in Chinese).

Zhang, X., Wang, Q. P., Ma, X. L., Zhang, X. P., Cheng, W., and Xia, Y. C.: The Influence of New Round-Trip Drifting Sounding Observation on the Quality of Numerical Prediction in the Middle and Lower Reaches of the Yangtze River, Chinese J. Atmos. Sci., 49, 245–256, https://doi.org/10.3878/j.issn.1006-9895.2304.22224, 2025b (in Chinese).

Zhang, X. F., Li, L. X., Yang, R. K., Guo, R., Sun, X., Luo, J, P., Chen, H. B., Liu, D. X., Tang, K. B., Peng, W. W., Han, X. D., Guo, Q. Y., Li, X. X., and Fei, X. K.: Comprehensive Marine Observing Experiment Based on High-Altitude Large Unmanned Aerial Vehicle (South China Sea Experiment 2020 of the "Petrel Project"), Adv. Atmos. Sci., 38, 531–537, https://doi.org/10.1007/s00376-020-0314-1, 2021a.

Zhang, X. P., Guo, Q. Y., Yang, R. K., Ma, X. L., and Cao, X. Z.: Assimilation Experiment of Rainstorm in the Middle and Lower Reaches of the Yangtze River Based on "ascent-drift-descent" Sounding Data, Meteorol. Mon., 47, 1512–1524, https://doi.org/10.7519/j.issn.1000-0526.2021.12.007, 2021b (in Chinese).

Zhang, X. P., Sun, L., Ma, X. L., Guo, H., Gong, Z. R., and Yan, X. H.: Can the Assimilation of the Ascending and Descending Sections' Data from Round-Trip Drifting Soundings Improve the Forecasting of Rainstorms in Eastern China?, Atmosphere, 14, 1127, https://doi.org/10.3390/atmos14071127, 2023.

Zhou, X. S., Guo, Q. Y., Xia, Y. C., and Tian, H.: Inspection of FY-3D satellite temperature data based on horizontal drift round-trip sounding data, J. Appl. Meteor. Sci., 34, 52–64, https://doi.org/10.11898/1001-7313.20230105, 2023 (in Chinese).

Zhou, X. S., Hong, G., Xia, Y. C., Luo, H. W., Bao, W. Z., and Tian, H.: Verification of FY-3D Satellite Humidity Profiles Using Descending Phase Data of Round-Trip Drifting Sounding, Meteor. Mon., 50, 1373–1385, https://doi.org/10.7519/j.issn.1000-0526.2024.063002, 2024 (in Chinese).

Zhu, H. J., Li, F. Z., Kan, Z. P., He, H., Xiao, D. E., and Zhang, L. Q.: Analysis of Buoyancy Change of Latex Balloon and Simulation of Vertical Trajectory, China Rubber Industry, 68, 17-24, https://doi.org/10.12136/j.issn.1000-890X.2021.01.0017, 2021 (in Chinese).

Zhuang, Z. R., Wang, R. C., Wang, J. C., and Gong, J. D.: GRAPES_Meso background error characteristics and application, J. Appl. Meteorol. Sci., 30, 316–331, https://doi.org/10.11898/1001-7313.20190306, 2019 (in Chinese).